Journal of Photochemistry and Photobiology C: Photochemistry Reviews 24 (2015) 16–42

Contents lists available at ScienceDirect

Journal of Photochemistry and Photobiology C: Photochemistry Reviews

journal homepage: www.elsevier.com/locate/jphotochemrev

Review

Review of material design and reactor engineering on TiO_2 photocatalysis for CO_2 reduction

Oluwafunmilola Ola*, M.Mercedes Maroto-Valer

Centre for Innovation in Carbon Capture and Storage (CICCS), School of Engineering and Physical Sciences, Heriot-Watt University, Edinburgh EH14 4AS, United Kingdom

ARTICLE INFO

Article history:
Received 25 February 2015
Received in revised form 19 May 2015
Accepted 10 June 2015
Available online 23 June 2015

Keywords:
Co_2 photoreduction
Photocatalysis
Photocatalytic reactor
Solar fuel production
Titanium dioxide
Artificial photosynthesis

ABSTRACT

The continuous combustion of non-renewable fossil fuels and depletion of existing resources is intensifying the research and development of alternative future energy options that can directly abate and process ever-increasing carbon dioxide (CO_2) emissions. Since CO_2 is a thermodynamically stable compound, its reduction must not consume additional energy or increase net CO_2 emissions. Renewable sources like solar energy provide readily available and continuous light supply required for driving this conversion process. Therefore, the use of solar energy to drive CO_2 photocatalytic reactions simultaneously addresses the aforementioned challenges, while producing sustainable fuels or chemicals suitable for use in existing energy infrastructure. Recent progress in this area has focused on the development and testing of promising TiO_2 based photocatalysts in different reactor configurations due to their unique physicochemical properties for CO_2 photoreduction. TiO_2 nanostructured materials with different morphological and textural properties modified by using organic and inorganic compounds as photosensitizers (dye sensitization), coupling semiconductors of different energy levels or doping with metals or non-metals have been tested. This review presents contemporary views on state of the art in photocatalytic CO_2 reduction over titanium oxide (TiO_2) nanostructured materials, with emphasis on material design and reactor configurations. In this review, we discuss existing and recent TiO_2 based supports, encompassing comparative analysis of existing systems, novel designs being employed to improve selectivity and photoconversion rates as well as emerging opportunities for future development, crucial to the field of CO_2 photocatalytic reduction. The influence of different operating and morphological variables on the selectivity and efficiency of CO_2 photoreduction is reviewed. Finally, perspectives on the progress of TiO_2 induced photocatalysis for CO_2 photoreduction will be presented.

Contents

* Corresponding author at: School of Engineering and Physical Sciences, Heriot-Watt University, Edinburgh, United Kingdom.
E-mail address: O.O.Ola@hw.ac.uk (O. Ola).

http://dx.doi.org/10.1016/j.jphotochemrev.2015.06.001

Dr Oluwafunmilola Ola joined the Centre for Innovation in Carbon Capture and Storage at Heriot-Watt University as Research Associate in CO_2 conversion and solar fuels. She is currently working on an EPSRC funded project to engineer novel photoreactors that can achieve efficient hydrocarbon conversion and separation from CO_2 for solar fuel production. Prior to this, she obtained MSc. (with distinction in Environmental Engineering at the University of Nottingham in 2010 and Ph. D. in Chemical Engineering at Heriot-Watt University. Her work on solar fuel production from CO_2 has resulted in over 25 (7 journals and 19 conference papers) publications that have been cited over 46 times. She is also a reviewer for 3 journals (Catalysis Science and Technology, Renewable Energy and ChemCatChem). Her contribution to this research field within the interface of materials chemistry and chemical engineering has led to the award of 10 travel grants and prizes such as RSC Energy Sector Ph.D. Thesis Award, RSC Solar Fuels Symposium Best Poster Prize, UKERC 3rd Place Poster Award and Engineering Research Showcase Highest Merit for Poster Presentation Award.

Prof M. Mercedes Maroto-Valer is the first Robert Buchan Chair in Sustainable Energy Engineering at Heriot-Watt University. This is a joint appointment between the School of Engineering and Physical Sciences and the Institute of Petroleum Engineering. At Heriot-Watt, she is the Head of the Institute for Mechanical, Processing and Energy Engineering (School of Engineering and Physical Sciences) and leads the pan-University Energy Academy. She is also Director of the EPSRC funded Centre for Innovation in Carbon Capture and Storage (CICCS). She is a member of the Directorate of the Scottish Carbon Capture and Storage (SCCS).She obtained a BSc with Honours (First Class) in Applied Chemistry in 1993 and then a Ph.D. in 1997 at the University of Strathclyde (Scotland). Following a one-year post-doctoral fellowship at the Centre for Applied Energy Research (CAER) at the University of Kentucky in US, she moved to the Pennsylvania State University in US, where she worked as Research Fellow and from 2001 as Assistant Professor and became Program Coordinator for Sustainable Energy. She joined the University of Nottingham as Reader in 2005 and within 3 years she was promoted to Professor in Energy Technologies. During her time at Nottingham she was the Head of the Energy and Sustainability Research Division at the Faculty of Engineering.She has over 300 publications, including editor of 3 books, 90 refereed publications in journals and book chapters and over 200 contributions to other journals and conference proceedings. She holds leading positions in professional societies and editorial boards, including FRSC, Chair of the RSC Energy Sector, Member of the Scientific Advisory Committee of the RCUK Energy Programme and of the UKERC Research Committee and Editor-in-Chief of Greenhouse Gases: Science and Technology.Her outstanding contributions, publication record and service to the chemical sciences and energy engineering have been recognized with numerous international prizes and awards, including 2013 Hong Kong University William Mong Distinguished Lecture, 2011 RSC Environment, Sustainability and Energy Division Early Career Award, 2009 Philip Leverhulme Prize, 2005 U.S. Department of Energy Award for Innovative Development, 1997 Ritchie Prize, 1996 Glenn Award—Fuel Chemistry Division of the American Chemical Society and the 1993 ICI Chemical & Polymers Group Andersonian Centenary Prize.

1. Introduction

1.1. Scope of the review

The pressures arising from the need for improved living standards triggered mainly by economic and population growth have detrimental effects on the environment through the continuous consumption of finite fossil fuel reserves linked to increasing CO_2 emissions [1,2]. The need to meet global energy demand predicted to increase due to a rising global population has led to the development of different strategies by which CO_2 emissions can be reduced. These can be achieved through the use of non-fossil fuels such as hydrogen, renewable and nuclear energy, increased energy efficiency, reduced deforestation and capture and storage of CO_2 emissions or by using a combination of these options. Although nuclear energy can supply low carbon energy, there are concerns with regards to waste generation [3,4]. Public acceptance and limited water availability are also key issues associated with this technology. There are several challenges, including capital cost, source and seasonal availability, economic barriers, geographical distribution and environmental issues as major constraints in the use of renewable energy like biomass, hydropower, solar and wind energy [1,5].

Conversely, the use of hydrogen energy eliminates the constraints associated with environmental impacts, but requires full optimization and energy input as its production is mainly from steam reforming and water electrolysis. Additional drawbacks are related to storage and hydrogen fueling infrastructures such as fuel

cell vehicles and fueling stations which are still being developed [6]. Carbon dioxide capture and storage (CCS) serve as a means of reducing CO_2 emissions, where CO_2 is removed and captured from large point sources of industrial processes, such as petrochemical plants, power generation, cement, iron and steel production and others. This is followed by its subsequent transport, injection and storage in various sinks, such as geological storage (underground saline aquifers, depleted oil and gas reservoirs and deep coal seams), mineral carbonation and ocean storage. The CO_2 separated and captured is then considered to be stored for prolonged periods ranging from centuries to millions of years [7]. Although the technologies associated with CO_2 capture and separation show great potential with regards to reducing cost and energy penalty [8], they still require further development. Bachu et al. compared the aforementioned storage options and identified geological storage as the preferable option owing to the significant quantity of CO_2 that can be sequestered, long retention time and great depth of experience from the oil and gas industry that would accelerate the immediate deployment after full-scale implementation [9]. CCS still needs optimization in order to fill the gap in knowledge with regards to the location and capacity of possible geological locations and possible leakage that could occur during or after injection. Public acceptance has also been recognized as a key factor that can pose barriers to the implementation of geological storage as the public can accelerate CCS development [9,10].

As CCS is still in the demonstration phase and may be uneconomical for emissions from small to medium sized sources, other sustainable alternatives with little or no environmental impacts and zero CO_2 emissions need to be developed. These technologies which can offset the cost associated with CO_2 capture and utilize CO_2 for chemicals and fuels production rely solely on technological breakthroughs and market competitiveness due to their versatile applications. At present, utilization of CO_2 accounts for approximately 2% of emissions and forecasts predict 700 megatons of CO_2/year could be mitigated [11]. Alternatives processes such as photocatalysis, direct photolysis, and electrochemical reduction can utilize CO_2 as opposed to geological storage [12,13]. The separated CO_2 stream from the capture plant will serve as a feedstock for these conversion methods. The synthesized products such as methane, methanol, ethanol etc., can be used as chemicals, feedstock in fuel cells or hydrogen sources for electricity. Mikkelsen et al. have highlighted the difference between photocatalysis and electrochemical reduction as the source of electrons which is obtained from irradiating semiconductors under light in the former and the application of an applied current in the latter [14]. Although electrochemical cells can convert CO_2, Yano et al. reported low efficiencies resulting from the deactivation of electrodes as a major drawback. This is due to the deposition of poisoning species, i.e., adsorbed organic compounds, on the electrode [15,16]. The need for an inexpensive hydrogen source and high energy photons have been reported as drawbacks in direct hydrogenation and photolysis [17,18].

In this review, CO_2 utilization by direct catalytic conversion of CO_2 driven by light energy is described. Although CO_2 conversion to energy rich and chemically useful products is endothermic, renewable carbon free sources like solar energy provide readily available and continuous light supply required for driving this conversion process under ambient conditions. Thus, carbon based fuels and chemicals suitable for end-use infrastructure can be produced from the conversion of CO_2 and water by semiconductor photocatalysts capable of simultaneously driving chemical reactions and utilizing solar energy. These value added products can be used directly or supplement feed stocks in hydrocarbon production or chemical processes. Amongst semiconductor photocatalysts, titanium dioxide (TiO_2) has been frequently used for UV induced photocatalysis due to its abundance, low cost and chemical stability. However, its use is limited due to its large band gap; as it can only be activated by ultraviolet (UV) light which represents 2–5% of sunlight [19]. Attempts to improve the efficiency of this catalyst for CO_2 photocatalysis are limited to the overall process efficiency being largely dependent on two factors—the physicochemical properties of the catalyst and reactor configuration. The optical and electronic properties of TiO_2 can be modified through the addition of metals or their oxides such as Cu [20], Ag [21], Pd [22] and Rh [23] and non-metals, such as nitrogen [24] and iodine [25]. When these metal and non-metal atoms occupy the interstitial sites, replace Ti in the substitutional sites or form aggregates on the surface of TiO_2, they can cause changes in the properties of TiO_2 [26], where the band structures and properties of TiO_2 have been reported to be tailored by this process. These metals also serve as a source of charge-carrier traps which can increase the life span of separated electron–hole pairs, and thus enhancing the efficiency and product selectivity for CO_2 photoreduction [13]. Furthermore, the textural properties such as the surface and bulk crystal structure, particle size and morphology can also be modified. However, it still remains largely unknown how the interaction of metal dopants or their oxides modify the surface chemistry and reaction mechanism of TiO_2 for CO_2 photoreduction. The configuration of catalyst particles in a photoreactor system is also another factor that can influence the overall photocatalytic efficiency of TiO_2 [27,28]. This review discusses the current conditions, limitations, correlations and possibilities of existing systems i.e., photocatalysts and reactors. The concept and mechanism of CO_2 photocatalysis using titanium dioxide (TiO_2) is presented in Section 1. Section 2 is focused on the route by which the physicochemical properties of TiO_2 can be modified. The influence of different operational variables i.e., reductant, temperature, pressure and particle size, on the photoactivity of TiO_2 is addressed in Section 3 while Section 4 reviews various techniques for the fabrication of immobilized semiconductor photocatalysts. Section 5 covers different catalyst configurations by which the textural properties of TiO_2 can be enhanced. Section 6 describes the current conditions, limitations and possibilities of existing photoreactor configurations available for CO_2 photocatalysis. Comparative analyses of existing systems crucial to the field of CO_2 photocatalytic reduction are discussed under Sections 4–6. Finally, Section 7 summarizes the review with future projections required for driving the field of CO_2 photocatalysis.

1.2. CO_2 photocatalysis

Since CO_2 is a chemically stable compound due to its carbon–oxygen bonds (bond enthalpy of C=O in CO_2 is +805 kJ/mol), its conversion to carbon based fuels requires substantial energy input for bond cleavage [29]. Renewable carbon free sources like solar energy provide readily available and continuous energy supply required for driving this conversion process. CO_2 photocatalysis offers the possibility of utilizing captured CO_2 to synthesize chemicals and fuels with the aid of semiconductor catalyst(s) under light irradiation. Apart from solar energy, other readily accessible light sources can be used. Fig. 1 highlights the typical photocatalytic process showing band gap formation in a typical semiconductor photocatalyst when exposed to light radiation. As shown in Fig. 1, the band gap is the energy region extending from the bottom of the empty conduction band (CB) to the top of the occupied valence band (VB). When an electron excited by light energy migrates from the fully occupied valence band of the semiconductor located at an energy level (Ev) to a higher energy (Ec) empty conduction band, electron–hole pairs are created if the absorbed light energy (hv) is greater than or equal to the band gap (Eg) of the semiconductor [12,30]. Eq. (1) presents the formation of

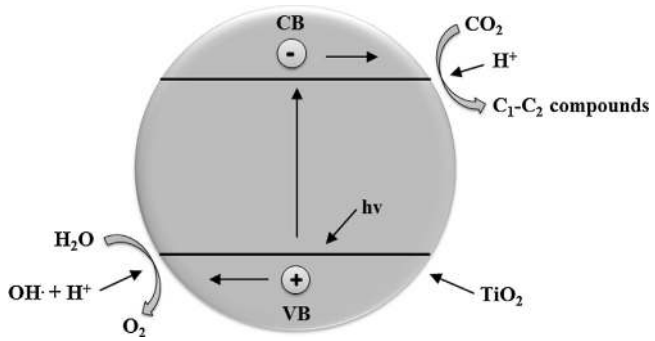

Fig. 1. Schematic of TiO_2 photocatalyzed reaction where CB and VB represents the conduction band, and valence band, respectively.

electron–hole pairs [31] where e^-, hv and h^+ represents the conduction band electron, photon energy and hole in the valence band, respectively.

$$\text{Photocatalyst} \xrightarrow{h\nu e^- + h^+} \quad (1)$$

$$e^- + h^+ \rightarrow \text{heat} \quad (2)$$

$$Eg = Ec - Ev \quad (3)$$

Eq. (2) shows that the charge carriers may also recombine in the surface or bulk before reacting with adsorbed species, dissipating energy as heat or light while Eq. (3) shows the band gap energy (Eg) which is equal to the difference between the energy of the conduction (Ec) and the valence band (Ev). The reduction potential of photo-generated electrons is the energy level at the bottom of conduction band while the energy level at the top of valence band determines the oxidizing ability of photo-generated holes which determine the ability of the semiconductors to undergo oxidations and reductions [19]. The redox potential levels of the adsorbate species and the band gap energy determine the likelihood and rate of the charge transfer processes for electrons and holes [32]. For an electron to be donated to the vacant hole, the redox potential level of the donor is thermodynamically required to be above the VB position of the semiconductor, while that of the acceptor should be below the CB position. The reduction potentials for CO_2 photoreduction with H_2O to various products with reference to NHE at pH 7 are given in Eqs. (4)–(13) below [33,34].

$$2H^+ + 2e^- \rightarrow H_2 \quad E^0 = -0.41 \quad (4)$$

$$H_2O \rightarrow \frac{1}{2}O_2 + 2H^+ + 2e^- \quad E^0 = 0.82 \quad (5)$$

$$CO_2 + e^- \rightarrow CO_2^{\bullet} \quad E^0 = -1.90 \quad (6)$$

$$CO_2 + H^+ + 2e^- \rightarrow HCO_2^{\bullet} \quad E^0 = -0.49 \quad (7)$$

$$CO_2 + 2H^+ + 2e^- \rightarrow CO + H_2O \quad E^0 = -0.53 \quad (8)$$

$$CO_2 + 4H^+ + 4e^- \rightarrow HCHO + H_2O \quad E^0 = -0.48 \quad (9)$$

$$CO_2 + 6H^+ + 6e^- = CH_3OH + H_2O \quad (10)$$

$$CO_2 + 8H^+ + 8e^- \rightarrow CH_4 2H_2O + H_2O \quad E^0 = -0.24 \quad (11)$$

$$2CO_2 + 8H^+ + 12e^- = C_2H_4 + 2H_2O \quad (12)$$

$$2\,CO_2 + 9H^+ + 12e^- \rightarrow C_2H_5OH + 3H_2O \quad E^0 = -0.33 \quad (13)$$

The band gaps of some of the most commonly used photocatalysts are shown in Fig. 2 [35–38]. Although some of these semiconductor photocatalysts such as hematite (Fe_2O_3) are low cost and possess suitable band gap energies for visible light absorption, they suffer from different limitations. Metal chalcogenides semiconductors e.g., CdS, PbS, CdSe etc., have been reported as being susceptible to photocorrosion and low stability especially in aqueous media [31,39]. The addition of sulphide or sulfite to the contacting solution has been described to suppress photocorrosion. These semiconductors have also been reported to show some toxicity [40]. Since semiconductors like WO_3, Fe_2O_3 and SnO_2 possess conduction band edge values below the

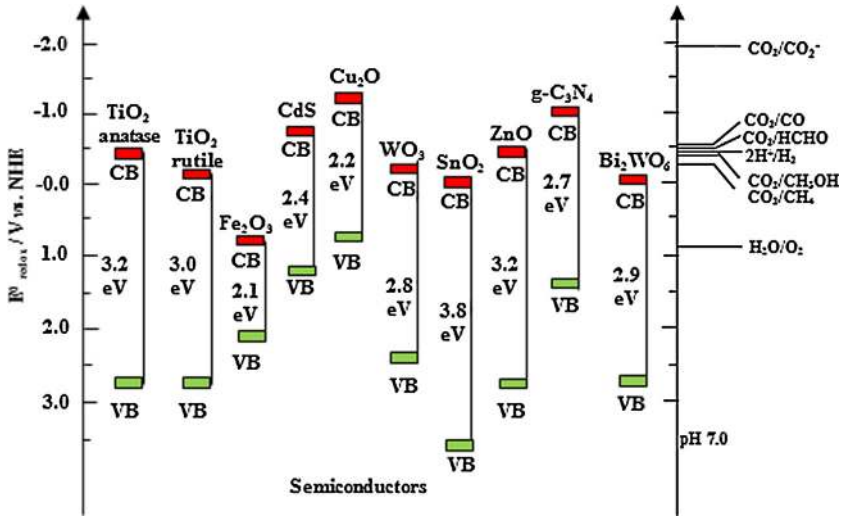

Fig. 2. Band gap of some photocatalysts with respect to the redox potential of different chemical species measured at pH of 7. Adapted from Refs. [35–38].

hydrogen potential and Gupta and Tripathi pointed out the use of an external electrical bias as a requirement needed to achieve hydrogen evolution during water splitting [41]. Fe_2O_3 has also been reported by Fox and Dulay to show lower photoactivity compared to TiO_2 and ZnO due to corrosion or the formation of short lived ligand-to-metal or metal-to-ligand charge transfer states [42]. The formation of $Zn(OH)_2$ on the surface of the semiconductor ZnO observed from its dissolution in water has been reported by Bahnemann et al. to cause instability and deactivation over time [43]. On the other hand, TiO_2 appears to be corrosion resistant and chemically stable [19].

Jeyalakshmi et al. also stated that large band gap semiconductors like TiO_2 are more suitable for CO_2 photoreduction due to sufficient positive and negative redox potentials in the VB and CB, respectively, compared to smaller band gap semiconductors like CdS where the energy levels of either the VB or CB tend to be unsuitable for water oxidation and/or CO_2 photoreduction [44]. The photogenerated electrons and holes may recombine to generate heat energy or become trapped in surface sites, where reactions with electron accepting or donating species adsorbed on the surface of the semiconductor photocatalyst can occur [30,45]. For redox reactions to take place, electron–hole recombination must be minimized.

Several researchers have studied CO_2 photoreduction using different semiconductors, including single catalysts like TiO_2 [46] and ZrO_2 [47], double catalysts like Cu–Fe/TiO_2–SiO_2 [48] and Cu–ZnO/Pt–$K_2Ti_6O_{13}$ [49], metal and compound oxides such as CuO [50], $LaCoO_3$ [51], Ga_2O_3 [52] and $ATaO_3$ where A represents Na, Li and K [53]. The basic characteristics of an ideal semiconductor photocatalyst were reviewed by Refs. [13,54–59]. These properties include the presence of a large surface area, cost-effectiveness, accessibility, resistance to photocorrosion or production of toxic by-products and the ability of the redox potentials of the photogenerated valence band and conduction band to be positive and negative in order for the electrons to act as an acceptor and donor, respectively. The most frequently used semiconductors are ZnO, CdS, TiO_2, WO_3 and NiO. However, compared to these semiconductors, TiO_2 still remains the most researched semiconductor photocatalyst due to its availability, chemical stability, low cost, high photocatalytic activity and resistance to corrosion.

1.3. TiO_2

The most common crystalline phases of TiO_2 are rutile, anatase and brookite. The bulk properties of the crystalline forms of TiO_2 are presented in Table 1. Anatase and rutile have lattice parameters (a and c) of 0.3733/0.4584 nm and 0.9370/0.2953 nm, respectively, in the unit cell based on the body centered tetragonal structure. The anatase form is the most suitable for photocatalytic reactions due to its larger surface area, stability and higher activity compared to the rutile form [60–63]. The brookite form is not commonly accessible, difficult to synthesize and has not been proved for photocatalytic reactions [64], [65]. Bouras et al. reported that optimal photocatalytic efficiency can be obtained from a mixture of anatase with a small percentage of rutile through a synergistic effect between the two crystalline phases as electron hole recombination is prevented by the creation of energy wells which serve as an electron trap formed from the lower band gap of rutile [62]. Although TiO_2 has several unique features, its use is limited due to its large band gap (see Table 1); as it can only be activated by ultraviolet light which represents 2–5% of sunlight [54,66]. Since visible light accounts for 45% of the solar spectrum [51,67], there is a need to develop titania based photocatalysts which are active under the visible light spectrum.

2. Modified TiO_2 catalysts

Since the time scale of electron–hole recombination of TiO_2 has been reported to be higher than the desirable redox reactions [33], it is crucial to modify the physicochemical properties of TiO_2 to improve process efficiency. Suitable modification of the optical and electronic properties of TiO_2 results in not only the reduction of the band width via the incorporation of addition energy levels but increased lifetime of the photogenerated electrons and holes via effective charge carrier separation and suppression of electron–hole recombination. Furthermore, the textural properties such as the surface and bulk crystal structure, particle size and morphology can also be modified. The photocatalytic activity of TiO_2 for visible light can be increased by using organic and inorganic compounds as photosensitizers (dye sensitization), coupling semiconductors of different energy levels or doping with metals or non-metals to suppress recombination rate and thus increasing quantum yield [54,56,68,69]. Table 2 highlights a summary of literature on CO_2 photoreduction using TiO_2 modifications [20,22,25,70–121]. All these strategies are described below.

2.1. Dye sensitization

Dye sensitization is a means of increasing absorption toward the visible light region through the inducement of the photo-excited dye molecule [19,56,122,123]. Various dyes which harvest visible light that have been used as sensitizers include rhodamine B, porphyrins, thionine, rose bengal, erythrosine B etc. [124–126]. Electrons are transferred from the dye molecule to the conduction band of the semiconductor when the energy level of the dye molecule was more negative than the semiconductor. Fig. 3 and

Table 1
Structural properties of crystalline structures of TiO_2.

Properties	Crystalline forms		
	Anatase	Rutile	Brookite
Crystalline structure	Tetragonal	Tetragonal	Rhombohedral
Lattice constants (nm)	$a = b = 0.3733$ $c = 0.9370$	$a = b = 0.4584$ $c = 0.2953$	$a = 0.5436$ $b = 0.9166$ $c = 0.5135$
Bravais lattice	Simple, Body centred	Simple, body centred	Simple
Density (g/cm^{-3})	3.83	4.24	4.17
Melting point (°C)	Turning into rutile	1870	Turning into rutile
Boiling point (°C)	2927[a]	–	–
Band gap (eV)	3.2	3.0	–
Refractive index (n_g)	2.5688	2.9467	2.8090
Standard heat capacity, C°p	55.52	55.60	–
Dielectric constant	55	110–117	78

[a] Pressure at pO_2 is 101.325 KPa.

Table 2
Modifications of TiO_2 for CO_2 photoreduction.

Modifications	Photocatalyst	Light source	Reductant	Products	References
Dye sensitization	Dye sensitized (perylene diimide derivatives) Pt impregnated on TiO_2	75 W daylight lamp	H_2O	0.74 μmol/g_{catal} CH_4	[70]
	N3 dye (Ru^{II}(2,2′-bipyridyl-4,4′-dicarboxylate)$_2$–Cu (0.5 wt%)–Fe (0.5 wt%)/TiO_2	Solar concentrator	H_2O vapor	0.617 μmol/g_{catal} h CH_4	[71]
	Ru/RuO_x sensitized TiO_2	Solar simulator	H_2O	900 μL h^{-1} CH_4	[72]
	N719/TiO_2	300 W Xe lamp	H_2O/2 M NaOH	0.1781 mmol/cm^2 CH_3OH 0.1292 mmol/cm^2 CH_2O	[73]
Semiconductor coupling	CdSe quantum dot (QD)-Pt/TiO_2 films	300 W Xe arc lamp, ≤100 mW/cm^2	H_2O	48 $ppmg^{-1}$ h^{-1} CH_4, 3.3 $ppmg^{-1}$ h^{-1} CH_3OH	[74]
	23.2 wt% AgBr–TiO_2	150 W Xe lamp	0.2 M $KHCO_3$	128.56 μmol g CH_4 77.87 μmol g CH_3OH 13.28 μmol g C_2H_5OH 32.14 μmol g CO	[75]
	PdS quantum dot (QD)-Cu/TiO_2	300 W Xe lamp	H_2O	0.82 μmol g^{-1} h^{-1} CO 0.58 μmol g^{-1} h^{-1} CH_4 0.31 μmol g^{-1} h^{-1} C_2H_6	[76]
	CdS/TiO_2 nanotubes Bi_2S_3/TiO_2 nanotubes	500 W Xe lamp	0.8 g NaOH 2.52 g Na_2SO_3	159.5 μmol g/catal CH_3OH 224.6 μmol g/catal CH_3OH	[77]
	CeO_2/TiO_2 SBA-15	300 W Xe lamp	H_2O	<12mmol/g catal CH_4	[78]
	45 wt% CdS/TiO_2	125 W Hg lamp	H_2O	~16 μmol g/catal CH_3OH ~3 μmol g/catal CH_3OH	[79]
	TiO_2/ZrO_2	8 W Hg lamp	0.2 mpl/L NaOH	~16 μmol g /catal CH_4 ~175 μmol g /catal H_2	[80]
	GaP/TiO_2	1500 W Xe lamp	H_2O	118 μM/g_{catal} CH_4	[81]
Metal doping	0.5 wt% Ru–TiO_2	100 W Hg lamp	1 M 2-propanol	200 μmolg-Ti^{-1} CH_4 ~250 μmol g-Ti^{-1} H_2	[82]
	TiO_2 pellets	UVC lamp	H_2O vapor	0.16 μmol/h H_2 0.25 μmol/h CH_4	[83]
	1 wt% Ag–TiO_2	Solar concentrator	H_2O vapor	4.12 μmol/g_{catal} h CH_3OH	[84,85]
	3 wt% CuO–TiO_2	6 (10 W) UV lamps, 2450 μW/cm^2	H_2O	2655 μmol/g_{catal} CH_3OH	[20,86]
	2 wt% Cu–TiO_2	8 W Hg lamp	0.2 M NaOH	1000 μmol/g_{catal} CH_3OH ~20 μmol O_2	[87,88]
	TiO_2 pellets	3 UVC lamps	H_2O	0.25 μmol h^{-1} CH_4	[89]
	5.2 wt% Ag–TiO_2	300 W Hg lamp	0.2 M NaOH	>10 μmol/g_{catal} CH_4 + CH_3OH	[90]
	0.15% Pt–TiO_2 nanotubes	8 W Hg lamp	H_2O	4.8 μmol h^{-1}/g Ti^{-1} CH_4	[91]
	Pd/RuO_2/TiO_2	450 W Xe short arc lamp	0.05 M NaOH 0.05 M Na_2SO_3	72 ppm $HCOO^-$	[92]
	2 wt% Pd–TiO_2	500 W Hg lamp	H_2O	24.7×10^{-8} mol CH_4	[22]
	2 wt% Cu–TiO_2-SBA 15	400 W halide lamp	0.1 M NaOH and H_2O	627 μmol g^{-1} h^{-1} CH_4	[93]
	0.5 wt% Cu/TiO_2–SiO_2	Xe arc lamp, 2.4 mW/cm^2	H_2O	60 μmol g^{-1} h^{-1} CH_4, 10 μmol g^{-1} h^{-1} CO	[94]
	Kaolinite/TiO_2	8 W Hg lamp	0.2 M NaOH	4.5 μmol g_{catal} CH_4, 2.5 μmol g_{catal} CO, ~5 μmol g_{catal} H_2	[95]
	0.1 wt% Y–TiO_2	300 W Hg lamp	0.2 M NaOH	384.62 μmol g_{catal} HCHO	[96]
	1 wt% and 3 wt% Ce–TiO_2 SBA 15	450 W Xe lamp	H_2O	1 μmol g^{-1} CO	[97]
	3 wt% Ag–TiO_2	8 W Hg lamp	H_2O	~100 μmol/g_{catal} H_2 ~6 μmol/g_{catal} CH_4 ~14 μmol/g_{catal} C_3H_6	[98]
	Ni–TiO_2 (0.1 mol%)	6 (3W/cm^2) UV lamps	H_2O	14 μmolg_{catal} CH_4	[99]
	La_2O_3/TiO_2	300 W Xe Lamp	H_2O	4.57 μmol CH_4	[100]
	CeF_3–TiO_2	500 W Xe lamp	H_2O	162 μmolg_{catal} CH_3OH	[101]
	1.5 wt% NiO–TiO_2	200 W Hg lamp	H_2O	19.51 μmol/g_{catal} h CH_3OH	[102]
	8.7 at% Pt/9.6 at% Cu–TiO_2	AM 1.5G solar simulator	H_2O	>180 ppm/cm^2 h H_2 49 ppm/cm^2 h CH_4 <25ppm/cm^2 h CO	[103]
	Ce–TiO_2	8 W Hg lamp	0.2 N NaOH	16 μmol/g_{catal} CH_4 750 μmol/g_{catal} H_2	[104]
	Pt/TiO_2	500 W Xe Lamp	H_2O	389.2 ppm H_2 277.2 ppm CH_4 12.4 ppm C_2H_6 785.3 ppm O_2	[105]
	Ti-KIT-6/Si-Ti = 100	300 W UV lamp	H_2O	4.14 μmol/g_{catal} h CH_4 2.55 μmol/g_{catal} h H_2 1.45 μmol/g_{catal} h CO	[106]
	Pt/$SrTiO_3$–Rh/Pt/$CuAlGaO_4$ WO_3	AM 1.5G	2 mM $FeCl_2$/$FeCl_3$	0.52 μmol CH_3OH 0.12 μmol H_2 ~5 μmol O_2	[107]
	Pt/$SrTiO_3$–Rh/Pt/$CuAlGaO_4$ WO_3	AM 1.5G	2 mM $FeCl_2$/$FeCl_3$	8 μmol/g CH_3OH ~1 μmol/g H_2 12 μmol/g O_2	[108]
	Degussa P25 TiO_2	1000 W Xe lamp	H_2O		[109]

Table 2 (*Continued*)

Modifications	Photocatalyst	Light source	Reductant	Products	References
				0.1 μmol/h CH_4 1.4 μmol/h H_2 2.7 μmol/h CO	
	$Ag/BaLa_4Ti_4O_{15}$	400 W Hg lamp	H_2O	0.7 μmol HCOOH 10 μmol H_2 22 μmol CO 16 μmol O_2	[110]
	CeO_2/TiO_2	500 W Xe lamp	H_2O	2.75 μmol/g h H_2/CH_4 1.28 μmol/g h O_2	[111]
	$Pt/MgO/TiO_2$ nanotubes	300 W Hg lamp	0.1 mol/L $KHCO_3$	100.22 ppm/h cm^2 CH_4 10.4 ppm/h cm^2 CO	[112]
	In/TiO_2	500 W Hg lamp	H_2O	244 $\mu molg^{-1} h^{-1}$ CH_4 81 $\mu molg^{-1} h^{-1}$ CO	[113]
	TiO_2 (20%)/KIT6	300 W lamp	H_2O	44.56 μmol/g H_2 44.56 μmol/g CH_4 1.09 μmol/g CH_3OH 120.54 μmol/g CO	[114]
Non-metal doping	N doped TiO_2/Ni	15 W UV lamp/ incandescent lamp	0.2 mol/L NaOH and Na_2SO_3	482 $\mu molg_{catal}$ CH_3OH	[115]
	N doped TiO_2/Pt–Cu	AM 1.5 outdoor sunlight, 75–102 mW/cm^2	H_2O	111 ppm/cm^2 h (CO,H_2, etc.)	[116]
	N doped TiO_2 nanotubes	500 W tungsten/ halogen lamp	0.1 N NaOH	1132.6 $\mu molg_{catal}$ CH_3OH 921.6 $\mu molg_{catal}$ HCHO 12475.8 $\mu molg_{catal}$ HCOOH	[117]
	C doped TiO_2	175 W Hg lamp	Na_2SO_3	2610.98 $\mu molg_{catal}$ HCOOH	[118]
	I doped TiO_2	450 W Xe lamp	H_2O	2.4 $\mu molg^{-1} h^{-1}$ CO	[25]
	TiO_2/N-100	–	H_2O	23 $\mu molg^{-1} h^{-1}$ CH_3OH	[119]
	g-C_3N_4–N–TiO_2 (CT–70)	300 W Xe Lamp	H_2O	14.73 μmol CO	[120]
	N–TiO_2/spirulina	13 W lamp	H_2O	144.99 μmol/g H_2 0.48 μmol/g CH_4 0.12 μmol/g C_2H_4 0.17 μmol/g C_2H_6	[121]

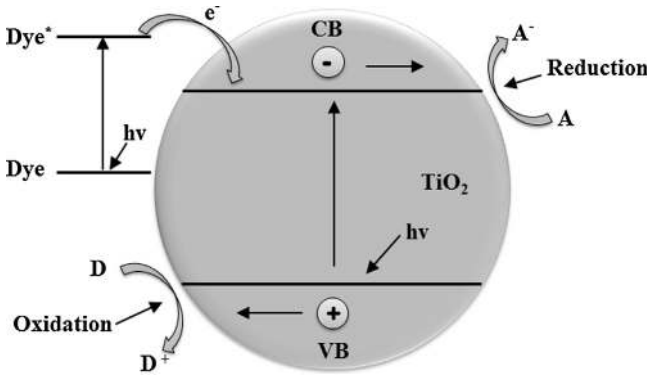

Fig. 3. Excitation steps with a photosensitizer, where A and D represent the electron acceptor and electron donor, respectively.

Eqs. (14)–(16) illustrate the reactions involved, including photo-excitation, injection of electrons and regeneration of dyes, respectively [122].

$$\text{dye} \rightarrow^{h\nu} \text{dye}^* \quad (14)$$

$$\text{dye} \rightarrow^{TiO_2} \text{dye}^+ + e^- \quad (15)$$

$$\text{dye}^+ + e^- \rightarrow \text{dye} \quad (16)$$

As shown in Fig. 3, the transferred electron reduces the organic electron acceptor (EA) adsorbed on the surface. An ideal photosensitizer must undergo slow backward reactions and fast electron injection to attain high efficiency [122]. The photosensitizer must also have high absorption spectrum in the visible light and infrared regions, with the excitation state having a long lifetime as well [69,127,128]. The rate of electron injection and back electron transfer reactions from the dye molecule to the photocatalyst depend on the characteristics of the dye molecule and the properties of TiO_2 and its interactions with the dye. Gupta and Tripathi [41] reported TiO_2 as an ideal semiconductor for dye sensitized solar cells due to its stability, high refractive index which facilitates increased light absorption, high dielectric constant for electrostatic shielding of the injected electron from the dye molecule to the electrolyte and suitable conduction band edge below the energy level of several dyes. Grätzel et al. conducted CO_2 photoreduction using Ru/RuOx sensitized TiO_2 and obtained approximately 900 μL h^{-1} of methane using a solar simulator with light intensity of 0.08 W cm^{-2} [72]. Ozcan et al. also demonstrated the effect of dye sensitized (perylene diimide derivatives) Pt impregnated on TiO_2 films on CO_2 photoreduction [70]. It was observed that methane production rate was enhanced to a maximum value of 0.74 $\mu mol/g_{catal}$ by adsorbing dye molecules to Pt–TiO_2. When Pt was not loaded on TiO_2 films, inactivity was observed in the presence of dye sensitizers. The N3 dye (Ru^{II}(2,2′-bipyridyl-4,4′-dicarboxylate)$_2$–$(NCS)_2$) coated with Cu–Fe/TiO_2 utilized by Nguyen et al. was found to be capable of visible light absorption, producing 0.617 $\mu mol/g_{catal}$ h of CH_4 after 5.5 h [71]. Data comparison between this sample and one without dye showed the stability of N3 dye sample over a wide light spectrum. Yuan et al. investigated the photoreduction of CO_2 with H_2O using a Cu(I) dye sensitized TiO_2 based system [129]. The introduction of the Cu(I) bipyridine complex was reported to be beneficial for charge separation in TiO_2 under full sun illumination (AM 1.5G). Maximum CH_4 production rate of ca. 7 $\mu mol/g^{-1}$ was observed following 24 h of visible light irradiation with no CH_4 detected when the pure Cu(I) dye complex was used. However, instability, light and thermal degradation of dye molecules and

disposal of undesired intermediates formed during reactions have been reported as a major drawbacks associated with dye sensitization [41,74,130].

2.2. Coupling of semiconductors

During heterojunction formation in semiconductor based photocatalysts, the direction of transfer of photogenerated charge carriers from the coupled semiconductors will depend on the position of the CB and VB. TiO_2 can be coupled with semiconductors via direct or indirect Z scheme. In direct Z-scheme, spatial charge separation occurs when electrons and holes are injected to CB and VB of different semiconductors in opposite directions (Fig. 4A), while charge separation does not occur in indirect Z-scheme due to electron and hole transfer occurring in the same direction for different semiconductors (Fig. 4B) [122,131–133]. The coupling of these semiconductors result in the balance of their Fermi levels (i.e., energy midway between the conduction and the valence band edges) such that electron flow is from the semiconductor with the higher Fermi level to the one with the lower Fermi level [134]. Excess negative charges are created in the semiconductor with the lower Fermi level while excess positive charges are created in the semiconductor with the highest Fermi level due to charge transfer. Thus, coupled semiconductors benefit from extended band widths in the visible light and increased charge separation. Sigmund et al. [134] reported that the injection of electrons or holes and their direction is dependent on the Fermi level and the band gap combination of the semiconductors. The requirements for successful coupling of semiconductors are efficient and fast electron injection; ability of the small band gap semiconductor to be excited by visible light with its conduction band being more negative than that of the other semiconductor; proper positioning of the Fermi energy level and insusceptibility of the semiconductors to photocorrosion [56,134].

Wang et al. [74] conducted studies of CO_2 photocatalytic reduction over CdSe quantum dot (QD) loaded with Pt impregnated TiO_2 films. Typical product yields of 48 ppm g^{-1} h^{-1} (methane) and 3.3 ppm g^{-1} h^{-1} (methanol) were observed in gas phase using visible light irradiation of 420 nm. They observed that charge injection into TiO_2 was facilitated by the shift of the conduction band of CdSe into higher energy which initiated CO_2 reduction. Process efficiency was also increased via charge separation due to electron transfer from CdSe to TiO_2. No activity was recorded when both semiconductors were used independently and using the same wavelength of light. Recently, ordered mesoporous silica SBA-15/TiO_2 composites with varying ratios of CeO_2 were synthesized by Wang et al. [78] for the reduction of CO_2 with H_2O under simulated solar irradiation. The addition of CeO_2 was found to not only influence the light harvesting properties of TiO_2 toward the visible

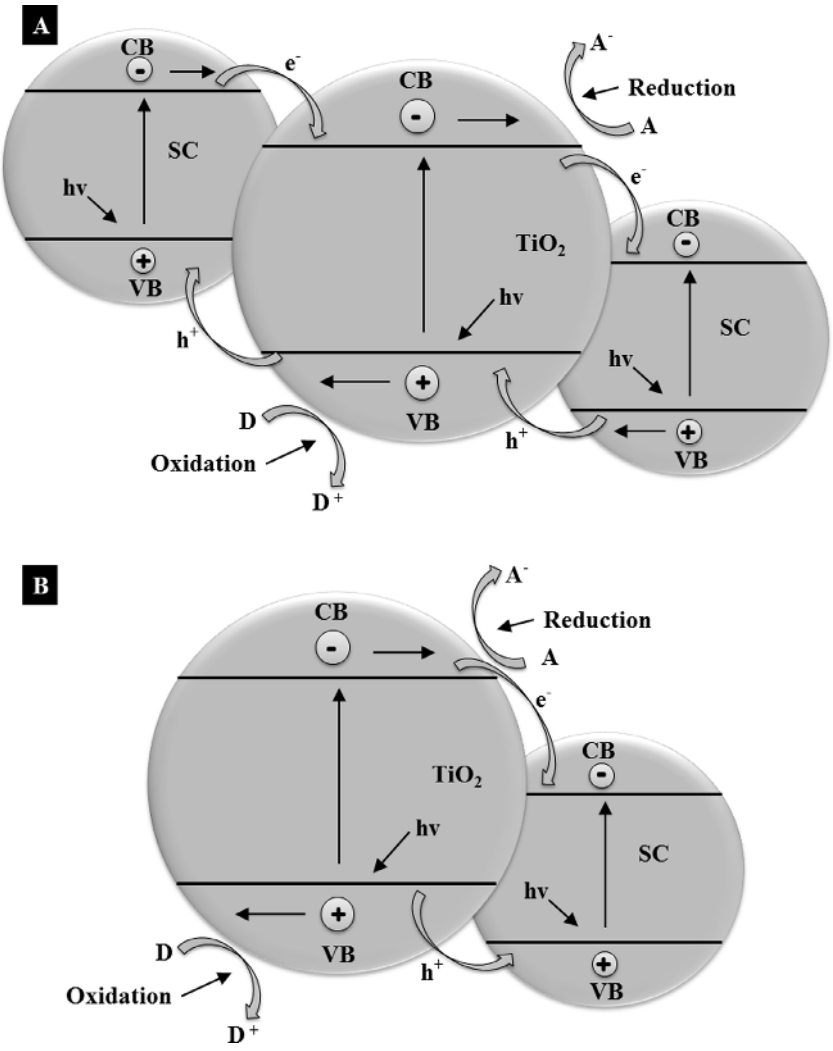

Fig. 4. Coupling of TiO_2 with semiconductors (SC) illustrating direct (A) and indirect (B) Z-scheme.

light region but enhance the photocatalytic performance as well. The improved performance was ascribed to the separation of photogenerated charge carriers induced from the drift of TiO_2 electrons to CeO_2.

Li et al. [77] utilized either CdS or Bi_2S_3 in the modification of the properties of TiO_2 nanotubes for CO_2 reduction under visible light irradiation. The addition of either semiconductor was found to enhance visible light absorbance and photocatalytic activity of TiO_2 nanotubes, with Bi_2S_3 exhibiting superior activity due to better surface area and CO_2 adsorption. Optimum methanol yields of 224.6 $\mu mol/g_{catal}$ and 159.5 $\mu mol/g_{catal}$ was observed using TiO_2 nanotubes coated with Bi_2S_3 and CdS, respectively. Heterojunction formation between the semiconductors was reported to play a crucial role in prolonging the lifetime of charge carriers and preventing electron/hole recombination. Despite its promising results, this technique is not widely applied due to its drawbacks. These include photo-corrosion in aqueous phase which affects the durability and stability of the catalyst through leaching out of dopant [135,136] and difficulty in finding appropriate semiconductor pairs such that recombination of charge carriers can be reduced [137].

2.3. Metal and non-metal modifications

The optical and electrochemical properties of TiO_2 can be enhanced by the addition of metal and non-metal ion(s). The band gap and properties of TiO_2 have been reported to be modified when metals or non-metals occupy non-lattice sites (i.e. interstitial), replace Ti in the substitutional sites or form aggregates on the surface of TiO_2 [26]. The redox potential of photogenerated charge carriers and visible light absorption will be determined by the spectral distribution of the modified photocatalysts, which is invariably determined by their chemical states [137]. Apart from these metals possessing their own catalytic activity, they also serve as a source of charge-carrier traps which can increase the life span of separated electron–hole pairs, and thus enhance the efficiency and product selectivity for CO_2 photoreduction [13,32].

Whether the metal ions are present in the lattice or TiO_2 surface is dependent on two key factors: the preparation procedure where the amount and homogeneity of the metal ions in its host oxide are key parameters and the firing temperatures to which the samples have been subjected. Diffusion of the metal ions in TiO_2 lattice is influenced by temperature; with higher temperatures favouring diffusion due to high thermal energy of the atoms. The mechanisms for metal and non-metal modification are described below.

2.3.1. Metal doping

Neamen [138] described doping as the process of adding foreign or impurity atoms into the crystal lattice of a semiconductor material. Alterations to the properties of the semiconductor can occur when controlled amounts of dopants are added to the semiconductor. Fig. 5 shows the schematic representation of these lattice defects. When these impurity atoms are located at normal lattice sites i.e., substitution of the host atom occurs, they are referred to as substitutional doping. Substitutional doping can occur when one or more of the following criteria are met: the differences in atomic radii of the atom types are less than 15%, dopant and host metals have similar crystal structures and electronegativity or comparable valences to ensure solubility [139,140]. Conversely, when these impurity atoms are present between normal lattice sites, they are referred to as interstitial doping i.e., the host atom dislodged from its normal lattice sites is forced into voids between atoms [138,139]. The likelihood of an atom occupying an interstitial site can be predicted by comparison of the radii of the interstitial dopant to the host metal [140]. The greater difference between these atomic radii results in the

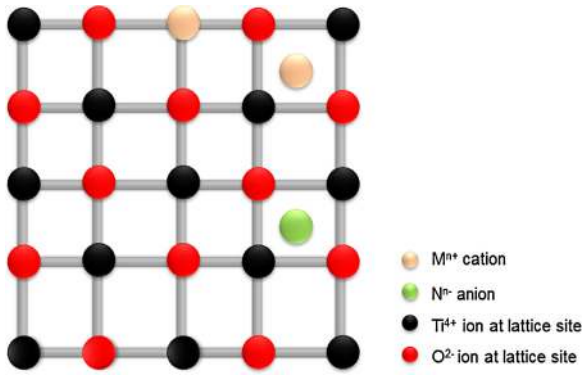

Fig. 5. Two dimensional representation of a single TiO_2 crystal lattice showing substitutional and interstitial doping.

dopants positioning itself in an interstitial site. The ionic radius ratio of the cation/anion (r^+/r^-) determines the preference of cations to occupy certain interstitial sites [140]. Interstitial sites may consist of cations with coordination numbers such as 4 (tetrahedral), 6 (octahedral) etc., based on the radius ratio of these ions. As the values of the ionic radius ratio increase, the number of anions packed around the cation increase. In tetrahedral holes, the cations are packed between planes of anions in close-packed structures if the ionic radius ratio falls within 0.225 and 0.414. Whilst the radius ratio falls within 0.414 and 0.732, if they are packed in octahedral holes [138].

According to Pagot and Clerjaud [141] and Seebauer and Kratzer [142], the local distortion of the crystal lattice can occur in substitutional and interstitial doping due to the difference in the atomic radii of the dopants compared with the host atoms and their chemical affinity with their surrounding atoms. In these lattice defects, the change in electric properties is caused by the disruption of the chemical bonding between the atoms and distortion of the geometric arrangement of atoms [138]. Vacancies may be created during the catalyst preparation process due to impurity atoms hopping from one vacancy to the other, thus remaining permanently in the substitutional lattice sites after calcination. Dopants can be introduced into sol–gel derived samples at molecular level through the mixing of titanium precursors with soluble dopant compounds. The introduction of dopants has been found to alter the degree of crystallinity and phase transformation, thereby, subsequently altering the peak heights, areas and relative intensities [143]. Phase transformation can be facilitated or inhibited by substitutional dopants when cations enter the anatase lattice and cause an increase or decrease in the level of oxygen vacancies through valence or reduction/oxidation effects. This leads to the subsequent rearrangement of atoms in the lattice of TiO_2 through the substitution of Ti^{4+} with cations. Conversely, the formation of Ti interstitials may distort the anatase lattice thus restricting the lattice contraction involved in the phase transformation to rutile [143]. The reactions of metal doping are described by the following equations, where M^n represents the metal ion dopant [56].

$$M^{n+} + h\nu \rightarrow M^{(n+1)} + e^-_{CB} \quad (17)$$

$$M^{n+} + h\nu \rightarrow M^{(n-1)} + h^+_{VB} \quad (18)$$

$$M^{n+} + e_{CB}{}^- \; M^{(n-1)+} \text{ as electron trap} \quad (19)$$

$$M^{n+} + h^+_{VB} \; M^{(n+1)+} \text{ as hole trap} \quad (20)$$

Eqs. (17) and (18) depict the formation of energy levels in the band gap of TiO_2, while (19) and (20) represent the transfer of electrons between TiO_2 and metal ions. However, the energy level ($M^{n+}/M^{(n-1)+}$) must be less negative than conduction band (CB) of TiO_2, while the energy level ($M^{n+}/M^{(n+1)+}$) must be less positive than valence band of TiO_2. The influence of iodine doping on the phase transformation and photocatalytic activity of TiO_2 for CO_2 reduction was evaluated by Ref. [25]. The anatase fraction of their iodine doped samples was found to increase with increased iodine concentration and calcination temperature while the brookite fraction was found to decrease under the aforementioned conditions. They attributed the optimal visible light activity of their 5 wt% I–TiO_2, calcined at 648 K sample to combinational effect of increased surface area, improved visible light absorption and enhanced charge separation from the substitution of Ti^{4+} with I^{5+} which led to the generation of titania surface states trapping electrons and suppressing recombination. The incorporation of substitutional or interstitial metal dopants in the titania structure generates trap levels in the band gap and thus modifying the band gap after doping. As shown in Fig. 6, the trap levels usually in the form of narrow bands are located below the lower conduction band edge. After modification, required energy level becomes $h\nu \geq (E_g - E_t)$ where E_t represents lower edge of the trap band level as opposed to $h\nu \geq E_g$ which is required for photon excitation before modification [134]. Consequently, electrons excited at these levels become trapped, with the holes having enough time for $OH^{\bullet}$ generation such that electron/hole recombination is suppressed and overall process efficiency improved. The choice of metal dopant is determined by the ability of the metal to exhibit multiple oxidation states, possess ionic radii and $M^{n+}/M^{(n+1)}$ energy levels closer to Ti^{4+} and the capacity to trap either electrons or holes.

The type of metal dopant added will determine whether the dominant charge carrier in the semiconductor will be either holes in the valence band or electron in the conduction band [138]. Koci et al. [12] reported doping as a means of increasing the level of holes in the band gap to permit the excitation of electrons where mobile holes are created in the valence band (p-type) or addition of an energy level fully occupied with electrons in the band gap which accelerates excitation into the conduction band (n-type). Carp et al. [19] described n-type and p-type dopants where the former acts as a donor centre of electrons and the latter conversely acts as acceptor centers of holes. Recombination centers are formed in p-type dopant as they have an affinity for hole formation once negatively charged, while electron–hole recombination in n-type occurs due to increase in concentration of conduction electrons.

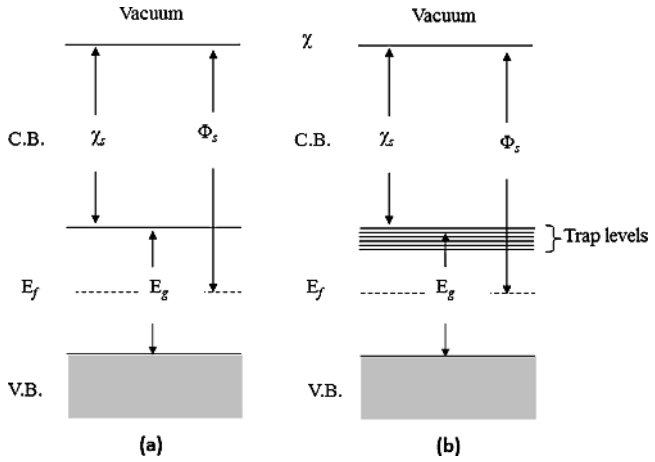

Fig. 6. Band structure of titania (a) before doping and (b) after doping where E_g,E_f, Φ, χ, and s represent the band gap energy, Fermi level, work function, electron affinity and semiconductor. Reprinted from Ref. [134] with permission.

They also reported that charge separation could be improved by co-doping to produce an overall beneficial effect.

Extensive studies on the improvement of the electronic structure of TiO_2 have been performed by doping with high energy transition metals by several researchers [130,144–147]. Their results established that the amount and type of metal dopant as well as the method of synthesis were key factors in determining photocatalytic activity and the extent of red shift that can be achieved in the visible light region. Comparisons between the absorption spectra of metal doped TiO_2 synthesized by chemical doping (impregnation) and metal ion implantation were made. Samples synthesized by the latter method exhibited shifts in their absorption band toward visible light region (~600 nm) caused by intense distance interaction between the metal ion and TiO_2. In contrast, the samples prepared by the impregnation method experienced no shift, but absorption shoulders in the UV/Vis spectra. This was caused by the creation of impurity energy levels with the amount of metal ions dopant used determining their intensity.

The electronic structure of TiO_2 doped with transition metals (Cr, Fe, Co, V, Ni and Mn) was also examined by Umebayashi et al. [148] using ab initio band gap calculations based on density functional theory. According to their work, a shift of the localized level to a lower energy was observed based on the increase of the atomic number of the dopant. Incorporation of metal or its oxide into TiO_2 structure has been reported to cause an increase in the recombination rate between photogenerated electrons and holes via the impurity energy level. Therefore, doping can be effective if the metal ions are placed near the photocatalyst surface where efficient charge transfer of the trapped electrons and holes can occur [41].

In the field of CO_2 photoreduction, Nie et al. [149] presented the formation of smaller particles as a way by which doping can alter recombination rate. As smaller particles have large surface to volume ratio, the migratory path is shorter such that the probability of the generated electrons and holes from the bulk undergoing recombination is reduced before reaching the surface. The dopant loading level plays a key role in CO_2 photocatalytic activity as increased product yield can be obtained due to red shift towards visible light [144]. However, doping at high concentrations results in the metal ions becoming recombination centres. Gupta and Tripathi [41] further explained that increasing doping concentration results in a narrowed space charge layer where electron–hole pairs within this region can be efficiently separated by the electric field before recombination. However, exceeding the optimum doping concentration results in an extremely narrow space charge layer such that light penetration depth exceeds the width of this space charge layer. Consequently, recombination rate increases due to the lack of a driving force to separate them.

Koci et al. [150] used different loading ratios of Ag/TiO_2 and observed an increase in product yield of methane and methanol, with 7% Ag/TiO_2 showing the highest product yield compared to lower loading ratios of 1%, 3% and 5%. Conversely, Sasirekha et al. [82] obtained an optimal Ru loading value of 0.5 wt%, after which photocatalytic activity decreased for 1.0 wt% due to increased electron–hole recombination. Slamet et al. [20,86] also reported that Cu dopant in excess of 3 wt% could reduce photocatalytic activity by reducing the depth of light penetration, and thus inhibiting interfacial charge transfer. When the doping content of Fe^{3+} exceeded 0.03 wt%, Xin et al. [151] recorded a decrease in photocatalytic activity due to electron–hole recombination, while the opposite was observed for lower loading content (<0.03 wt%).

Regarding product formation, extensive studies into the use of doped TiO_2 in CO_2 photocatalysis have been conducted using various metals such as chromium [152], copper [86,153], silver [154], platinum [91], palladium [155] and ruthenium [92]. Several

primary products with their yields includes methane (4.8 μmol h^{-1}/g_{Ti}^{-1} [91], methanol (2655 μmol/g_{catal} [86] and 4.12 μmol/g_{catal} [84] and formate (72.3 ppm [92]), respectively have been obtained. However, thermal instability and increase in recombination centers are drawbacks linked with this process [24,156].

2.3.2. Metal semiconductor modification

The overall efficiency and surface properties of a semiconductor can be altered by the addition of a metal which is not chemically bonded to TiO_2 [134]. These metals act as an electron scavenger and thus facilitate the generation of holes. Ren and Valsaraj [157] and Usubharatana et al. [13] described the addition of metals as a source of charge-carrier traps which increased the life span of separated electron–hole pairs and enhanced reaction rate. Fig. 7 illustrates the band structure of TiO_2 before and after contact with a metal. As shown in Fig. 7, the comparison of a semiconductor with work function Φ_s to a metal with work function $\Phi_m > \Phi_s$ results in the Fermi level of the semiconductor, E_{Fs} being higher than the Fermi level of the metal E_{Fm}. When this metal is brought in contact with TiO_2 (Fig. 7b), electrons will flow from the semiconductor to the metal until the two Fermi energy levels reach an equilibrium. This results in an upward band bending formed due to an excess of positive charges in TiO_2 generated from the migrating electrons [158]. Consequently, this bending at the metal–semiconductor interface creates a small barrier known as the Schottky barrier [32]. The Schottky barrier serves as an electron trap which prevents migrating electrons from crossing back to the semiconductor and thus preventing recombination. The schematic in Fig. 8 also illustrates the mechanism of a metal modified semiconductor for photocatalysis where recombination is

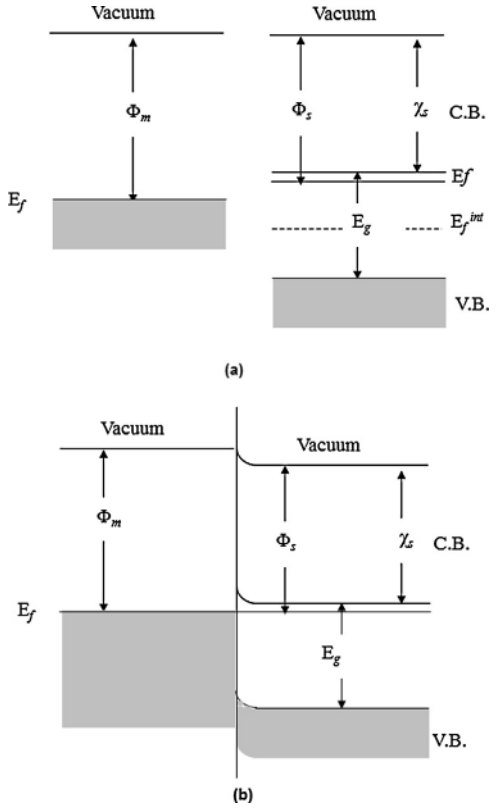

Fig. 7. Band structure of titania (a) before contact and (b) after contact with a metal, where the Schottky barrier is formed. (Φ_m and E_f^{int} represent the metal work function and Fermi level if titania is an intrinsic semiconductor respectively. Reprinted from Ref. [134] with permission.

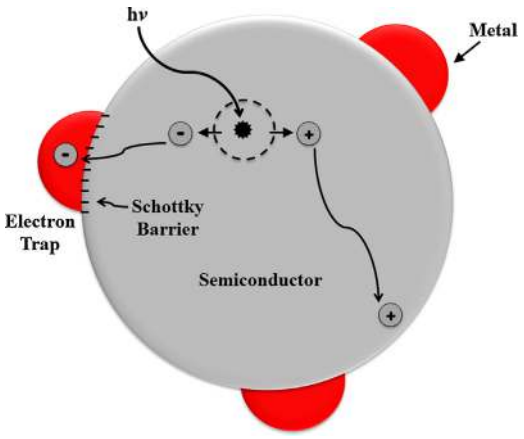

Fig. 8. Metal modified semiconductor photocatalyst.

suppressed by the Schottky barrier of the metal in contact with the surface of the semiconductor.

As a result of this trapping mechanism, the photogenerated electrons then diffuse to the surface of the adsorbed species where reduction takes place. Photoreactivity can be negatively influenced by either a high concentration of metallic islands on the semiconductor surface or an enhancement of their size [158]. When this occurs, reduced surface illumination of catalysts and increased recombination rate is observed. Krejcikova et al. [90] conducted CO_2 reduction studies using different loading ratios of $Ag/TiO_2$and observed increased product yield of methane in the gas phase and methanol in the liquid phase with increasing Ag concentration under 254 nm UV irradiation over a 24 h period. The increase in product yield compared to both commercial and synthesized pure TiO_2 was attributed to higher Fermi level of TiO_2 and Schottky barrier formation which facilitated electron transfer from the TiO_2 conduction band to Ag particles and improved charge separation, respectively. Tseng et al. [87] synthesized Cu loaded TiO_2 nanoparticles for the photocatalytic reduction of CO_2 under UV irradiation using NaOH as a reductant. CH_3OH production was found to increase with increasing Cu concentration, after which a markedly decrease was observed when the loading ratio exceeded 2 wt%. Optimum CH_3OH production of 118 μmol/g was obtained using the 2 wt% Cu–TiO_2 sample following 6 h of UV illumination. The formation of the Schottky barrier between Cu and TiO_2 and the electric charge redistribution via semiconductor–metal contact was reported to facilitate electron trapping and thus promoting improved photo-efficiency.

Other than Schottky barrier, loading of noble metals such as Ag [159], Cu and Au [160] on the TiO_2 can enhance visible light absorption via localized surface plasmonic resonance (SPR) effect. This phenomenon can occur either by collective oscillation of valence electrons in plasmonic nanostructures in resonance with electric field part of inbound radiation or metallic elements creating trap sites that propagates light within the semiconducting material [161]. Morphology and size of the plasmonic nanostructures influence the SPR frequency and intensity as well as the resonant wavelength. Gas-phase photochemical reduction of CO_2 using mesoporous TiO_2 modified with bimetallic Au/Cu nanostructures was studied for CH_4 production under UV irradiation [162]. The bimetallic nanocomposites were reported to exhibit higher activity (CH_4 yield of ~11 μmol/g_{catal}) compared to Au/TiO_2 and Cu/TiO_2 (CH_4 yield <4 μmol/g_{catal}).

2.3.3. Non-metal modification

Doping with non-metals creates heteroatomic surface structures and can modify the properties and activity of TiO_2 toward

visible light [137]. Some of the non-metals that have been used include nitrogen (N) [24], carbon (C) [118], sulphur (S) [163,164], fluorine (F) [165]. Asahi et al. [24] and Asahi and Morikawa [156] described doping with anions as being more efficient for photocatalytic activity compared to cations because they do not form recombination centers caused by the presence of *d* states deep in the band gap of TiO_2. Liu et al. [137] reported that effective band gap narrowing can only occur by anion dopants if the non-metal has a comparable radius with O atoms and lower electronegativities than O, with the aim of facilitating uniform distribution and elevating the valence band.

The band gap energy of TiO_2 has been reported to be narrowed by a mixture of p states of the non-metal dopant with the O 2p states of TiO_2 via substitutional or interstitial doping [24,156]. Conversely, Valentin et al. [166,167] proposed that substitutional doping with N results in the formation of localized levels within the band gap, with the catalyst synthesis conditions determining whether either interstitial or substitutional nitrogen exists in the lattice of TiO_2. On the other hand, Serpone et al. [168] attributed the origin of visible light absorption in their titania samples to the existence of color centers instead of band gap narrowing via mixing of states, as proposed by Liu et al. [137].

First principle calculations by Asahi et al. [24] using anions (F, N, P, S and C) indicated the superior activity of N owing to the p states influencing band gap narrowing through combination with O 2p states. Although S doping showed similar photoresponse as N, they found the ionic radius of S too bulky to be integrated into the lattice of TiO_2. Zhang et al. [25] tested iodine doped TiO_2 synthesized by the hydrothermal method and found that the calcination temperature influenced the rate of CO_2 photoreduction under visible light irradiation. They observed that increased calcination led to reduced surface area. An optimal yield of CO (2.4 $\mu mol\, g^{-1}\, h^{-1}$) was observed for the 10 wt% sample calcined at 375 °C. Xue et al. [118] examined carbon doping for CO_2 photoreduction using citric acid as the carbon source and Na_2SO_3 as the reductant. After 6 h irradiation using high pressure 175W mercury lamp, 2610.98 $\mu mol/g_{catal}$ of CH_2O_2 was produced. This was significantly higher than the undoped TiO_2.

Compared to other non-metals, N doped TiO_2 ($TiO_{2-x}N_x$) has been extensively studied because of its photoactivity toward visible light [137,169]. Zhao et al. [117] prepared N doped TiO_2 nanotubes via hydrothermal method at different calcination temperatures. N doping into TiO_2 nanotube framework was found to be effective for increasing the photoactivity of TiO_2 in the visible light region compared to pure TiO_2 and N doped TiO_2. Optimum total organic carbon content (sum of the product yields of formaldehyde, methanol and formic acid) of 14,530 $\mu mol/g_{catal}$ was observed using a N–TiO_2 nanotube sample calcined at 500 °C for CO_2 reduction with 0.1 N NaOH as reductant following 12 h of light irradiation.

Since its quantum efficiency of anion doping is still low, investigations have been conducted by codoping with metals to enhance the reaction rate [170,171]. Several transition metals such as Pd, Fe and Pt have been used in the photodegradation of pollutants and dyes [172–174]. The results of these researchers showed the increased photocatalytic activity and absorbance of visible light by the metal ion modified $TiO_{2-x}N_x$ compared to bare $TiO_{2-x}N_x$. CO_2 photoreduction studies have been carried out by Varghese et al. [116] using N–TiO_2 nanotube arrays with metals (Pt and Cu) under outdoor AM 1.5 sunlight. They found the optimal nitrogen concentration to be 0.75 atom% with Cu doping generating greater hydrocarbon product yield of 104 ppm/ (cm^2 h) compared to Pt doping. As both Pt and Cu have varying effects toward product selectivity; the combination of both metals resulted in an optimal yield of 111 ppm/cm^2 h.

2.3.4. Co-doping

The properties of TiO_2 can also be modified via co-doping, which can be achieved via the combination of metal/metal, non-metal/metal or non-metal/non-metal pairs. A synergistic effect can be obtained with an appropriate combination of co-dopants compared to their single ion doped or undoped TiO_2 [128]. During co-doping, the non-metal can cause a red shift in the visible light region, while the metal can facilitate the transfer of photogenerated charge carriers thus suppressing recombination. Apart from co-dopants facilitating band gap narrowing, their combination can result in the formation of different heterostructures (i.e., different electronic structures) with respect to TiO_2 [44]. A heterostructure consisting of different combinations of non-metal and metal has the capacity for improved charge separation (metal) and visible light absorption (non-metal). Factors crucial for successful co-doping are the selection of the compatible co-dopants and the method of introducing the dopants which affects the doping level [44]. Several metallic and non-metallic combinations such as N–I [175], C–vanadium (V) [176] and Ag–V [177] have been used in the photodegradation of pollutants and dyes. The results of these researchers showed the increased photocatalytic activity and absorbance of visible light by the metal combinations compared to un-doped and single doped TiO_2 systems.

For metallic combinations for CO_2 reduction, the catalytic activity of sol–gel derived Mn–Cu/TiO_2 nanocomposites of varying metal concentrations was evaluated by Richardson et al. [178]. After 24 h of UV irradiation, the photocatalytic activity of CO_2 using 0.1 M NaOH and 0.25 M $KHCO_3$ was found to be promoted based on the coupling of Mn and Cu doped titania photocatalysts compared to either commercial TiO_2–P25 or single metal loaded samples. Improved results were due to electron transport to the dopant which suppressed electron/hole recombination. Maximum CH_3OH yield of 238.6 $\mu mol/g_{catal}$ was achieved using the 0.22 wt% Mn/0.78 wt% Cu–TiO_2 sample. The same trend was observed in a further study conducted by Richardson et al. [179] using different sol–gel derived Cu–Ga/TiO_2 nanocomposites of varying metal concentrations. The photocatalytic activity was improved when Cu and Ga doped photocatalysts were used such that the 0.78 wt% Cu/0.22 wt% Ga–TiO_2 sample gave the maximum HCHO yield of 394 $\mu mol/g_{catal}$ when compared to single metal loaded samples or TiO_2–P25. They reported that their optimized results were due to the rapid transfer of high energy electrons in their catalytic structures.

For metallic and non-metallic combinations in CO_2 reduction, co-doped N and Ni were introduced onto TiO_2 framework for CO_2 reduction using 0.2 mol/L of NaOH and Na_2SO_3 [115]. An increased red shift toward the visible light was observed using the co-doped samples compared to pure titania and individually doped samples of Ni–TiO_2 and N–TiO_2. An optimal methanol yield of 482 $\mu mol/g_{catal}$ was observed after 8 h of UV light irradiation using the 4 wt% N–6 wt% Ni/TiO_2 sample compared to the methanol yield of the individually doped samples of 245.4 $\mu mol/g_{catal}$ of 4 wt% N–TiO_2 and 214.4 $\mu mol/g_{catal}$ of Ni–TiO_2. They suggested that improved activity was due to the improved properties (surface area and crystallinity) of the co-doped samples and the synergy created by the metal (Ni) acting as an electron trap and the non-metal (N) facilitating increased visible light absorption.

Li et al. [180] demonstrated that co-doped mesoporous Pt–N/TiO_2 photocatalysts had some inherent advantages over undoped TiO_2. Using the optimum loading ratio of 0.2 wt% Pt for the synthesis of the co-doped samples under NH_3 atmosphere, they observed increased CH_4 evolution rate with increasing nitridation temperature up to 525 °C. After this temperature was exceeded; a subsequent decrease in CH_4 evolution was observed. Optimal CH_4

production rate of ca. 2.6 μmol/g_{catal}^{-1} was observed using the 0.2 wt% Pt–TiO_2 sample when the amount of doped N was 0.84% on the basis of lattice oxygen atoms under visible light irradiation. Improved activity under increasing nitridation temperature was due to the doping of more N atoms in the lattice position of oxygen in TiO_2, which gave rise to improved visible light absorption. Above the optimum N doping concentration, decreased photocatalytic activity was observed due to increased defect sites and non-stoichiometry of the samples.

Co-doped samples were synthesized by Wang et al. [74] using commercial P25 TiO_2 nanoparticles and CdSe quantum dots (QDs). Pt was further incorporated by the wet impregnation methods onto the CdSe–TiO_2 samples for the experimental investigation for CO_2 reduction using H_2O. They found that the use of co-catalyst, Pt with CdSe quantum dot (QD)-sensitized TiO_2 heterostructures led to increased visible light absorption greater than their individual photoresponse. No photocatalytic activity was also observed when either CdSe or Pt doped on TiO_2 was employed for CO_2 reduction. However, the synergy between CdSe–Pt/TiO_2 heterostructures was found to influence methane and methanol production under visible light irradiation with wavelength of 420 nm. In order to further demonstrate the need for heterostructure formation in co-doped samples, Wang and co-workers synthesized PbS–Cu/TiO_2 samples with different sizes of quantum dots. Although they achieved optimal activity with the 4 nm co-doped heterostructure, the drawback of photocorrosion observed from oxidation in their previous and current studies could not be surmounted. Zhang et al. [181] prepared co-doped Cu/I–TiO_2 samples with different concentrations using wet impregnation and hydrothermal methods. Under UV–vis and visible light irradiation, the photoactivity of the co-modified sample was found to be higher than either of the single ion modified catalysts (Cu–TiO_2/I–TiO_2). For CO production under visible light, the optimum yield of 6.74 μmol/g^{-1} was observed on the 1 wt% Cu–10 wt% I–TiO_2 while the optimum yield of 12 μmol/g^{-1} was observed on the 0.1 wt% Cu–10 wt% I–TiO_2 sample under UV–vis light irradiation. The presence of the dopant was reported to reduce the crystal size and influence visible light absorption while Cu facilitated charge transfer and enhanced CO_2 reduction.

3. Influence of operating parameters on CO_2 reduction

The following operating parameters listed below have been shown to influence CO_2 photoreduction: type of reductant, temperature, pressure and particle size. These factors are discussed in the following sections.

3.1. Effect of reductant

Several types of reducing agents such as H_2O, NaOH, and C_3H_7OH amongst others have been tested for CO_2 photocatalytic reduction [182–184]. For CO_2 photoreduction using TiO_2 to become economically feasible, readily available sources of hydrogen are needed. H_2O still remains the most naturally abundant source of hydrogen that is available and inexpensive [13]. Other reductants such as NH_3, pure H_2 gas etc., which serve as hydrogen sources are not readily available as primary feedstock and require prior preparation [185]. However, the drawback of utilizing water is the low solubility of CO_2 in H_2O (2 g/L) and the competition of the CO_2 photoreduction process with hydrogen formation, as shown in Eqs. (4) and (6), which indicate that it is thermodynamically more favorable to reduce H_2O than CO_2 [33,186].

Liu et al. [182] investigated the role of solvents on the product selectivity for CO_2 reduction in an attempt to increase reaction yield. Their results indicated that the use of solvents with low dielectric constants, such as $CCCl_4$ and CH_2Cl_2, led to $CO_2^{\bullet-}$ anion radicals being strongly absorbed on Ti sites due to the anions showing little solubility in these solvents of low polarity and therefore, CO was the major product observed during this reaction. When a high dielectric solvent such as H_2O was used, $CO_2^{\bullet-}$ anion radicals were greatly stabilized by the solvents which led to weak interactions with the surface of the photocatalyst, and thus formate was observed, as the main product via the reaction of a proton with the carbon atom of the $CO_2^{\bullet-}$ anion radical.

Zhao et al. [187] employed titania supported cobalt phthalocyanine (CoPc) nanoparticles for CO_2 reduction in either NaOH or Na_2SO_3 solutions. Maximum production of formic acid and formaldehyde was observed at concentration of 0.15 M due to increased solubility of CO_2 in NaOH and the OH^- ions produced from NaOH acting as strong hole scavengers during the OH radical formation. They further explained that electron/hole recombination could be suppressed through the longer decay time of electrons, since the holes are preoccupied in HCO_3^- formation in the CO_2 saturated system. Further addition of an optimal concentration of Na_2SO_3 (0.1 M) led to an increase in formal acid production through increased hole scavenging and proton concentration within the semiconductor particle for CO_2 reduction. The same phenomenon was also observed by Tseng et al. [87] in their CO_2 reduction studies using NaOH solution.

The study conducted by Koci et al. [188] demonstrated the influence of the volume of reductant on CO_2 photocatalytic studies using TiO_2. The use of NaOH was reported to not only enhance CO_2 solubility, but also facilitate improved CO_2 reduction via OH^- radical formation, which promoted the longer decay time of electrons. The production rate of CH_4 and CH_3OH was found to increase when the volume of NaOH increased from 50 to 100 mL, and then markedly decreased above these values. For example, the CH_4 yield increased from 7.5 μmol/g_{catal} to >8 μmol/g_{catal} when the volume of NaOH increased from 50 to 100 mL, then decreased to <2 μmol/g_{catal} when 250 mL of NaOH was used. Ti-MCM-41 mesoporous photocatalysts with Si/Ti molar ratios of 50, 100 and 200 were tested for CO_2 photoreduction using NaOH, deionized H_2O and monoethanolamine (MEA) as reducing agents. For the best photocatalyst within the series tested (Ti-MCM-41 with Si/Ti ratio of 50), maximum CH_4 yield of 62.42 μmol/g_{catal} was observed when MEA was used as a reductant compared to 5.62 μmol/g_{cata} of CH_4 over H_2O after 8 h of UV illumination. The lowest CH_4 yield of 1.96 μmol/g_{catal} over NaOH was due to the formation and precipitation of sodium bicarbonate ($NaHCO_3$) in solution after contact with CO_2 gas stream. Although the use of solvents other than water as hole scavengers can increase product selectivity and yield, they still remain economically unsustainable due to their potential to increase cost.

3.2. Effect of temperature

CO_2 photocatalysis is generally conducted at ambient conditions, i.e., room temperature because solubility decreases with increasing temperature and the formation of electron/hole pairs occurs by photon (light energy) activation. An increase in reaction rate has been reported to occur at high temperatures due to increased collision frequency and diffusion rate [188]. The optimum temperature required for photocatalysis is within 293–353 K, with decreasing activity occurring outside this range [189]. This is due to exothermic adsorption of reactants being the rate limiting step as the temperature approaches the boiling point of H_2O. Yamashita et al. [190] demonstrated that photocatalytic reactions proceed more efficiently at temperatures higher than 275 K by using anchored titanium oxide catalysts for CO_2 reduction. They observed increased production rates of CH_4, CO and CH_3OH under UV irradiation at 323 K compared to 275 K. Saladin and Alxineit [191] studied the effect of temperature on CO_2

reduction using titania samples irradiated under UV light for 4 h. They found that the production rate of CH_4 increased when the temperature rises from 298 to 473 K. Based on model calculations, the reaction rate was not expected to be substantially improved after the maximum temperature of 473 K due to hindered absorption of reactants. They also concluded that thermal activation processes such as product desorption played a crucial role in improved reaction rate at 473 K. Product desorption readily occurred at higher temperatures (473 K) compared to lower temperatures (298 K).

Guan et al. [49] investigated the use of a hybrid catalyst Pt loaded potassium hexatitanate ($K_2Ti_6O_{13}$) combined with Fe based catalyst supported on Y zeolite (Fe–Cu–K/day) for CO_2 reduction under concentrated sunlight. They found that the $Pt/K_2Ti_6O_{13}$ catalyst produced H_2 from water decomposition, while the Fe–Cu–K/day catalyst reduced CO_2 with the resulting H_2 converted into CH_4, HCOOH and HCHO. The reaction temperature was found to promote the generation of the products listed above in addition to C_2H_5OH and CH_3OH over the hybrid catalyst on temperature increase from 534 to 590 K. They claimed that the simultaneous supply of photons and thermal energy from the solar concentrator was responsible for the optimal production of reaction products observed at 590 K. The same phenomenon with higher production rate was also observed by Guan et al. [192] when they used a hybrid catalyst Pt loaded potassium hexatitanate ($K_2Ti_6O_{13}$) combined with Cu/ZnO catalyst under concentrated sunlight at 583 K. Increased methanol yield on temperature increase within the range of 333–373 K was also observed by other researchers during CO_2 reduction studies [20,193].

Photoreduction studies conducted by Kaneco et al. [194] demonstrated that temperature had no effect on the catalytic activity of their samples. The photocatalytic activity of TiO_2 suspended in supercritical CO_2 was investigated. Formic acid production observed in the liquid phase was attributed to the reaction of water with reaction intermediates on the surface of TiO_2. An increase in temperature at the rate of 278 K from 308 to 323 K led to the steady state formation of formic acid. Koci et al. [188] reported that a temperature increase of 10 K from 299 K to 309 K did not influence the hydrocarbon production rate for the photocatalytic reduction of CO_2 using TiO_2 following 4 h of UV irradiation. Although increasing reaction temperatures have been reported to facilitate increased production rates, the cost of fabricating sophisticated high temperature photoreactor systems capable of maintaining the selected optimum temperatures and the source of thermal energy required to heat up solvents i.e., water has a high specific heat capacity, still poses a problem.

3.3. Effect of pressure

Improved product selectivity has been reported to occur due to increased CO_2 concentration resulting from an increase in CO_2 pressure in aqueous media [188]. Experimental studies conducted by Mizuno et al. [195] demonstrated the effect of CO_2 pressure on CO_2 reduction using TiO_2 suspensions in H_2O and NaOH. CH_4, C_2H_4 and C_2H_6 were observed in the gas phase under pressurized conditions (2500 kPa), with no hydrocarbon production detected under ambient pressure. CH_4 production was found to increase sharply with increased CO_2 pressure from 500 to 2500 kPa. Slight increase in formic acid production was observed in the liquid phase under similar pressurized conditions. Overall, increased CO_2 pressure accelerated CO_2 reduction when both H_2O and NaOH were used.

On the other hand, CHOOH and CH_3OH production was observed in the liquid phase at ambient pressure. While a linear increase of formic acid was observed with slight pressure increase, CH_3OH yield was found to reach an optimal rate at 1000 kPa. Overall, the gross amount of hydrocarbons produced in the liquid phase exceeded that of the gaseous phase. Similar trend of increased hydrocarbon production was observed when NaOH was used as the hole scavenger under CO_2 pressurized conditions. Additional reaction products such as C_2H_5OH and CH_3CHO were also detected in the liquid phase. They suggested that improved reaction yield was due to the availability of CO_2 on the surface of TiO_2, which accelerated CO_2 reduction.

Koci et al. [188] demonstrated that the pressure influenced the rate of product yield obtained. They observed that the amount of CH_3OH yield in the liquid phase increased when CO_2 pressure was increased from 110 kPa (0.75 $\mu mol/g_{catal}$) to 130 kPa (1.5 $\mu mol/g_{catal}$). Further pressure increase to 140 kPa led to reduced CH_3OH yield. Conversely, CH_4 yield in the gas phase increased with increasing CO_2 pressure from 120 kPa (2.75 $\mu mol/g_{catal}$) to 140 kPa (4.5 $\mu mol/g_{catal}$). Kaneco et al. [186] studied the photocatalytic reduction of CO_2 under various pressures using TiO_2 suspended in *iso*-propyl alcohol medium. The results show that the pressure increase from 200 to 2800 kPa can increase CH_4 production linearly. Conversely, the increased pressure conditions were found to inhibit CHOOH production, with reaction product observed at only 750 kPa. The lack of C_2H_4 formation was attributed to the accelerated formation of CH_4. An increase in CH_3OH formation from 175 to 230 μmol/g-cat was observed by Tseng et al. [87] when the CO_2 pressure increased from 110 kPa to 125 kPa. Further pressure increase above 125 kPa led to decreased CH_3OH production rate of 85 μmol/g-cat. Cost of fabricating sophisticated high pressure systems must be considered when selecting parameters for reactor designs in CO_2 reduction.

3.4. Effect of particle size

Particle size is a key parameter in photocatalytic processes since the interaction between the amount of absorbed and reflected photons and the reactants depends on it. Apart from nanostructured photocatalyst possessing high surface area, they also benefit from low refractive index which minimizes light reflection, high surface to volume ratio and rapid charge transfer [196,197]. Several researchers have established that photocatalysts in the form of nanoparticles are more effective than bulk powders [198–200]. The rate of electron–hole recombination has been reported to be controlled by particle size since extremely small ultrafine particle (within the diameter range of few nanometres) experience surface recombination as opposed to large particles where volume recombination predominates [200]. The problem of volume recombination can be overcome by reducing the particle size. During surface recombination, most of electron–hole pairs photogenerated close to the surface undergo rapid recombination due to their shorter migratory paths, abundant surface trapping sites and limited driving force for charge separation [138]. This phenomenon has been reported to occur within certain size reduction. Zhang et al. [200] further demonstrated that the number of available active surface sites and transfer rate of surface charge carrier increased with smaller particle sizes due to their larger surface area. They observed increased photoactivity in the decomposition of $CHCl_3$ when TiO_2 particle size decreased from 21 to 11 nm. Decreased photoactivity was also observed when the particle was further reduced to 6 nm. Optimal photoactivity was demonstrated with the 10 nm particle. On the other hand, Koci et al. [198] proposed that the 14 nm TiO_2 particle was the optimal value for CO_2 reduction, since they obtained maximum CH_4 and CH_3OH production using this particle size. A decrease was observed on further increase to 29 nm. They attributed the decreased photoactivity observed in samples with particle size $<$14 nm to rapid flocculation which decreased availability of active sites.

The model developed by Almquist and Biswas [199] was used to elucidate the effect of particle size on TiO_2 activity for the photo-oxidation of phenol. Particle sizes ranging from 5 to 165 nm were prepared from flame synthesized TiO_2 and commercially available P25 and anatase TiO_2. The results also highlighted the strong dependence of particle size on photo-activity. Increased photo-oxidation occurred when the particle size increased from 5 to 30 nm and decreased when the particle size increased beyond this value. The optimal particle size range reported was within the range of 25–40 nm. Band gap of photocatalysts has been reported to be influenced by particle size [41,138,197]. They proposed that semiconductor particles within the nanometre range experienced energy shift according to the size quantum effect which could accelerate reduction and oxidation reactions via the conduction and valence band, respectively. This size quantization effect expected to cause an increase in the band gap energy results in a shift to larger redox potentials, which increases rate constants for surface charge transfer. Banerjee [201] also reported that the large fraction of surface atoms and high surface to volume ratio found in nanoparticles are responsible for enhanced light absorption through indirect electron transition at the boundary of the crystal i.e., surface or interface between two crystals. Particle size of photocatalysts must be carefully considered during catalyst synthesis since it is invariably linked to surface area and photocatalytic efficiency.

4. Catalyst configuration: supports

TiO_2 can be synthesized as powders (nanospheres, microspheres), crystals, films or immobilized by dip or spin coating onto substrates such as fibers, membranes, glass [202], monolithic ceramics [155], silica [203] and clays such as zeolite [204], kaolinite [95], montmorillonite [205] etc. Several materials have been used as TiO_2 support for CO_2 reduction. The use of supports eliminates the need for post treatment separation, provides high surface area and mass transfer rate [202]. The product selectivity, structure and electronic properties of TiO_2 can be modified by the use of supports. However, the photocatalyst must be strongly adhered to the support and have light absorption properties to be effective. An ideal support must be resistant to degradation induced by the immobilization technique and should provide firm adhesion between the support and the catalyst [206,207]. Mass transfer limitations and low light utilization efficiency due to little or no light absorption in the pores or channels of the catalyst coated supports are key limitations that have been identified with the use of supports [208]. Many researchers have focused on ways of anchoring photocatalysts onto supports since high photo-conversion efficiencies and improved light harvesting can only be achieved through the combined use of optimized photoreactor and photocatalyst configurations. An overview of some commonly used supports is presented below, including glass, optical fibers and monoliths.

4.1. Glass

Several types of glass substrates such as beads [209], plates [210], microfiber filter [94,98,211] and plates [102] have been used for CO_2 reduction due to the transparency of the substrates to light irradiation. The use of conductive materials like glass as supports have been extensively studied due to their ability to prevent total internal reflection through surface roughening which also provides better catalyst adhesion to the glass substrate and increases the amount of immobilized catalyst per unit area [28]. Furthermore, Ray and Beenackers [28] reported that utilizing conductive materials serve as a means by which light can be transmitted to the catalyst film which is connected to an external potential that can move excited electrons, and thereby, reducing electron–hole recombination to improve efficiency.

Highly dispersed titanium oxide anchored onto Vycor glass was tested for the photocatalytic reduction of CO_2 with H_2O [190]. The supports were prepared through facile reaction between surface OH groups of a transparent porous Vycor glass and $TiCl_4$. UV irradiation of the support led to the formation of C_1 compounds such as CH_4, CH_3OH and CO as major products and trace amounts of C_2 compounds (C_2H_4 and C_2H_6) at 323 K. Cu nanoparticles were deposited on transparent conductive fluorinated tin oxide (FTO) glass substrates for CO_2 reduction to CH_4 under UV irradiation [212]. Cu–TiO_2 films were reported to exhibit higher yields compared to pure TiO_2 and TiO_2 P25. Enhanced light absorption and increased diffusion length of photoinduced electrons were amongst some of the reasons for enhanced CO_2 photoconversion rates. TiO_2 pellets (Aerolyst 7708) were affixed to a flat glass tray by Tan et al. [83,89,213] to increase absorption capacity and contact area for CO_2 photoreduction. The product yield of CH_4 (200 ppm) using ultraviolet light C (UVC) wavelength of 253.7 nm was reduced to values lower than 100 ppm on switching to ultraviolet light A (UVA) wavelength of 365 nm after 48 h of irradiation.

Platinum (Pt)–TiO_2 nanostructured thin films with different deposition times were prepared by Wang et al. [213] for immobilized onto indium tin oxide (ITO)-coated aluminumosilicate glass using RF magnetron sputtering and gas-phase deposition method. The films which had a one-dimensional structure of TiO_2 single crystals with ultrafine Pt nanoparticles (NPs, 0.5–2 nm) were found to exhibit enhanced CO_2 photoreduction efficiency with selective CH_4 yield of 1361 $\mu mol/g_{catal}$ h. The fast electron-transfer rate in TiO_2 single crystals and the efficient electron–hole separation by the Pt NPs were the main reasons reported to be attributable for this enhancement. Mesoporous Cu–TiO_2 nanocomposites synthesized by a one-pot sol–gel method were loaded onto glass fiber filters as thick films for CO_2 photoreduction to CO and CH_4 [94]. CH_4 and CO peak production rates of 10 and 60 $\mu mol/g_{catal}$ h were achieved over the 0.5% Cu/TiO_2–SiO_2 composite. Improved results were reported to be influenced by the synergistic effect resulting from the combination of the SiO_2 substrate and Cu deposition loaded onto the glass fiber filter.

The effect of Ag/TiO_2 nanoparticles deposited on glass microfiber filter for UV light induced CO_2 photoreduction using water vapor as electron donor was performed by Collado et al. [98]. Deposition of Ag on TiO_2 surface led to an enhancement in the production of C_1–C_3 compounds which increased as Ag loading increased from 1.5–3.0 wt%. Better catalytic performance and selectivity were observed over glass filters containing Ag samples prepared by wet impregnation than incipient wetness impregnation procedure. Enhanced hydrocarbon production was reported to be due to lower recombination rates and synergistic effect between TiO_2 and Ag nanoparticles. The transparency of the glass material used can also limit the overall efficiency due to the catalyst receiving insufficient light e.g., Pyrex glass can cut off UV light below 300 nm [214]. On the other hand, quartz glass is a better alternative as a light conducting material because of its excellent light transmission properties and its ability for increased contact efficiency, thus creating more active sites.

4.2. Optical fibers

The use of a single or bundle of optical fibers for the remote delivery of light to reactive sites of coated photocatalysts has been studied by several researchers for wastewater treatment and CO_2 photocatalysis [48,154,215–217]. All researchers observed

increased degradation and conversion rates when the optical fibers were simultaneously used as a support and light distributing guide. In optical fiber, light is transmitted along the fiber core by the cladding with lower refractive index that traps light in the core through total internal reflection. Light can be primarily emitted at the end of the fiber (end emitting) or through the leakage of light as it travels from the fiber core to the cladding via the side surfaces (side emitting) [218].

Catalytic performance of 120 catalyst coated optical fibers was evaluated for CO_2 reduction under 365 nm UV irradiation. Maximum CH_3OH yield of 0.45 $\mu mol/g_{catal}$ h was achieved using 1.2 wt% Cu–TiO_2 catalyst coated fibers. Properties of the optical fibers such as external surface area and light transmittance were reported to influence the processing capacity of the catalysts. The influence of the optical fibers in delivering photons required to activate different catalyst combinations such as Cu–Fe/TiO_2, Cu–Fe/TiO_2–SiO_2 and N3 dye–Cu–Fe/TiO_2 was further demonstrated [48,71,219]. Overall, maximum CH_4 production rate of 1.86 $\mu mol/g_{catal}$ h was obtained using Cu (0.5 wt%)–Fe (0.5 wt %)/TiO_2–SiO_2 catalyst coated fibers while ethylene production rate of 0.575 $\mu mol/g_{catal}$ h was achieved with Cu (0.5 wt%)–Fe (0.5 wt%)/TiO_2 coated fibers under UVA irradiation. During gas phase CO_2 reduction studies, Wang et al. [193] obtained yields of 11.3 $\mu mol/g_{catal}$ h and 11.3 $\mu mol/g_{catal}$ h for methanol production under visible light irradiation and sunlight, respectively, when the optical fibers were coated with NiO/$InTaO_4$.

32 optical fibers coated with inverse opal Cu–TiO_2 inserted in a stainless tube were tested for the photoreduction of CO_2 to CH_3OH [157]. CH_3OH product rate of 0.036 $\mu mol/g_{catal}$ h was achieved after UV irradiation with light intensity of 113.65 mW/cm^2. The inverse opal configuration was reported to enhance catalyst activation via increased contact time of light within the photocatalyst. Although high catalyst loading and direct light excitation of coated catalyst films can be achieved when a bundle of optical fibers are coated, fragility of the optical fibers and the durability of their coatings has been described as drawbacks associated with their use [197]. The durability and performance of these fibers are directly related to the adhesion of the catalyst coatings on the fibers and thickness of the coated layer which may not withstand severe gas/liquid continuous flow conditions [220,221]. Even though roughening of the fiber surface has been reported to increase durability of these coatings, the problem of uneven catalyst and light distribution has also emerged [220,221]. Heat build-up from the bundled array of fibers can result in catalyst deactivation [222].

4.3. Monoliths

The use of interconnected three-dimensional structures like honeycomb monoliths containing parallel straight channels has been exploited for industrial processes due to its potentially high surface to volume ratio, easy of scale-up through an increase of its dimensions and channels, control of structural parameters (i.e., pore volume, pore size and surface area) etc. [223,224]. Different types of metal oxides and mesoporous materials have been immobilized on TiO_2 coated monolithic materials to improve catalytic performance for CO_2 photoreduction. Tahir and Amin [225] deposited montmorillonite (MMT) based TiO_2 onto monolithic structure to improve surface area and adsorption of gaseous species for CO_2 photoreduction with H_2O. The addition of MMT into TiO_2 matrix was reported to increase surface area from 42.98 m^2/g for pure TiO_2 to 51.79 m^2/g for MMT/TiO_2. Higher CO (52 $\mu mol/g_{catal}^{-1} h^{-1}$) and CH_4 (139 $\mu mol/g_{catal}^{-1} h^{-1}$) production was achieved over the MMT/TiO_2 monolith compared to pure TiO_2 (CO, 47 $\mu mol/g_{catal}^{-1} h^{-1}$ and CH_4, 82 $\mu mol/g_{catal}^{-1} h^{-1}$) after 10 h of UV light irradiation. Photocatalytic activity was reported to be influenced by increased CO_2 adsorption originating from surface hydroxyl (OH) groups in MMT/TiO_2 framework. The effect of monolithic geometry such as cell density and channel length on UV induced CO_2 photocatalysis was further evaluated. The product rates were reported to be influenced by the geometry of the monolith since maximum product rates of CO and CH_4 were observed over the monoliths with lower cell density of 100 cells per square inch (cpsi) and channel length of 2.5 cm compared to the monolith with higher cell density (400 cpsi) and lengths of 1.2, 1.7 and 5 cm. The monolith channel length was reported to be linked to light distribution. The effect of In loading on TiO_2 coated monoliths was further tested for photocatalytic reduction of CO_2 under UV irradiation by the same research group [226]. The introduction of indium to TiO_2 framework not only increased surface area and reduced particle size, but also facilitated charge transfer. Maximum CH_4 production rate of 55.4 $\mu mol\, g^{-1} h^{-1}$ was observed over 10 wt% In/TiO_2 monolith with 100 cpsi after 10 h of UV irradiation.

Photocatalytic studies conducted using monoliths as catalytic support for wastewater treatment, NO and CO_2 reduction have identified low light utilization efficiency due to little or no light absorption in the pores or channels of the honeycomb monolith as a major drawback associated with its use [155,208,223]. Not all immobilized photocatalyst may be activated due to limited light distribution arising from the catalyst coated on the outer surface absorbing most of the light and its intensity decaying rapidly along the opaque channels of the monolith [207,227]. In a

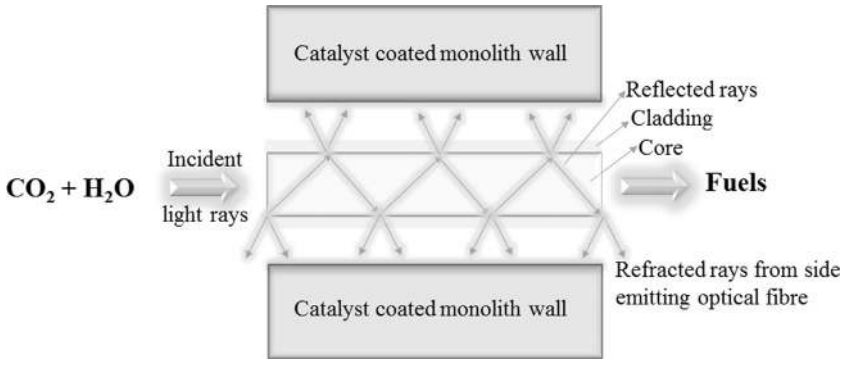

Fig. 9. Schematic of light propagation in a single channel of a coated honeycomb monolith threaded with a non-coated side light emitting optical fiber.

mathematical model developed by Hossain et al. [228] for influx of UV light within a square channel monolith, half of the incoming light flux was reported to be lost due to light shadowing effect at the entrance of the channel of the monolith wall. The UV light flux was also reported to decrease sharply with increasing distance in the monolith channel. A strategy for improving light distribution in monolithic structures was originally proposed by Du et al. [220], where non coated side-light emitting fibers were evenly distributed in each TiO_2 coated channel to ensure light refracted out of the surface of the fiber could reach the catalyst–reactant interface without attenuation. Fig. 9 shows the schematic where the gaseous reactants diffuse into each coated interconnected monolithic channel, adsorb and react with catalyst activated by a non-coated side-light fiber to form desorbed products and intermediates which diffuse back into the bulk gas stream (CO_2 saturated with H_2O).

In recent years, studies on CO_2 reduction using non coated side-light emitting fibers with geometric notches in the core–cladding system were reported to improve photocatalytic activity [229,230]. Vapor phase CO_2 with H_2O was reduced to CH_3OH by $NiO/InTaO_4$ coated monoliths containing no fibers, bare fibers and fibers with tip-reflection and mid-carves under visible light irradiation. Highest CH_3OH rate of $\sim$0.16 $\mu mol\,g^{-1}\,h^{-1}$ was observed over 1 wt% $NiO/InTaO_4$ monolith containing fibers with tip-reflection and mid-carves compared to the monolith containing no fibers and bare fibers. The results are linked with fibers with tip-reflection and mid-carves having the highest side light emission percentage of 98% compared to no fiber (84%) and bare fiber (93.8%) amongst configurations. Overall, maximum acetaldehyde conversion rate of 0.3 $\mu mol\,g^{-1}\,h^{-1}$ was achieved with the 2.6 wt% $NiO/InTaO_4$ monolith containing fibers with tip-reflection and mid-carves by simulated sunlight AM1.5G at 70 °C. The loading of different metal-based TiO_2 nanomaterials onto monolithic structures threaded with optical fibers were tested for UV and visible light induced CO_2 photocatalysis [102,230]. The loading of metal or metal oxide on the surface of TiO_2 via the introduction of defects into the lattice was reported to tailor its band width towards the visible light and alter its particle properties. For example, sol–gel derived 1 wt% Ni^{2+}-based TiO_2 monolith containing optical fibers showed improved CH_3OH production rate of 13 $\mu mol/g_{catal}\,h$ compared to pure TiO_2 coated monolith. Addition of Ni^{2+} influenced activity and selectivity of TiO_2 toward UV and visible light region due to the substitutional metal ions not only causing changes in the electronic structure and light absorption properties of TiO_2, but also altering the surface area, grain size and degree of phase transformation.

4.4. Other supports

The effect of co-catalyst (Cu–Pt)-sensitized TiO_2 nanoparticle wafer on CO_2 photocatalytic conversion was studied under full sun illumination (AM 1.5G) [103]. Coated wafers which had randomly connected pores were used as flow through membrane such that reactants (CO_2 and H_2O) pass through one end of the membrane and products collected at the other end. Improved product rates were achieved due to back reactions limited by the diffusion of reaction products to the outlet. Optimum amount of catalyst loading on the TiO_2 wafer were 9.6 at% Cu and 8.7 at% Pt. Hence, maximum conversion of CO_2 to CH_4 (49 $ppm/cm^2\,h$) was achieved over TiO_2 wafer sputtered with both Cu and Pt layers than Pt ($\sim$28 $ppm/cm^2\,h$) and Cu (38 $ppm/cm^2\,h$). Thin layer of CdS–TiO_2 nanocomposite was coated on a stainless steel support to improve CO_2 reduction performance. Performance of catalyst coated supports was dependent on metal concentration and size of the nanoparticles. Maximum CO and CH_4 production rates of 10.5 and 1.5 $\mu mol/g_{catal}$ under visible light irradiation were observed for the stainless steel support coated with 45% CdS–TiO_2 nanocomposite.

The direct conversion of CO_2 over TiO_2 coated stainless steel webnets of varying sizes was investigated under UV irradiation [231]. High surface area and good utilization of UV light were observed on TiO_2 films deposited on the webnets. An increase in mesh size resulted in increased TiO_2 surface area and reduced penetration of UV light. Evaluation of the photocatalytic activities of TiO_2 coated on three different mesh sizes of stainless steel webnets for CO_2 photoreduction resulted in higher product rate for TiO_2 coated on 120 mesh size than TiO_2 coatings on 60 and 200 mesh sizes. Nishimura et al. [232] dip coated TiO_2 on a silica–alumina gas separation membrane to obtain 3.5 ppmV/h of CO after 336 h, while Pathak et al. [233] used the hydrophilic structural cavities in Nafion-117 membrane films to host TiO_2 coated with nanoscale silver and obtained 0.071 mg^{-1} and 0.031 mg^{-1} of methanol and formic acid after 5 h. Reproducible results were obtained when these films were reused. Cybula et al. [234] employed a flat perforated steel or plastic tray as a support for the dispersion of TiO_2 in a tubular reactor designed for CO_2 photoreduction studies. They observed that the type of support used not only played a critical role in determining the amount of immobilized catalyst but also influenced the photoconversion rate when the same coating procedure was used. A decrease in catalyst loading and methane production (from 90 ppm to 34 ppm) was observed when the support was switched from steel to plastic due to weaker adhesion of TiO_2 on plastic compared to steel. CO_2 photoreduction studies by Shioya et al. [203] and Li et al. [94] employed silica as supports due to its even composition and orderly mesoporous structure with small channels. Sasirekha et al. [82], Yang et al. [93] and Li et al. [94] attempted to improve this arrangement by doping with metals such as Ru and Cu. They found that the combination of metals with mesoporous silica enhanced the reaction rate due to effective TiO_2 dispersion and improved absorption of CO_2 and H_2O on the surface of SiO_2. Product yields of 60 $\mu mol\,g\text{–}TiO_2^{-1}\,h^{-1}$ and 10 $\mu mol\,g\text{–}TiO_2^{-1}\,h^{-1}$ were obtained for CH_4 and CO, respectively, in a continuous flow photoreactor at an optimal doping ratio of 0.5 wt% Cu using Xe arc light source [94]. Maximum CH_4 production of 627 $\mu mol\,g^{-1}\,h^{-1}$ was observed by Yang et al. [93] with 2 wt% Cu after 8 h reaction time. Improved surface area and better dispersion of cerium (Ce)–TiO_2 on mesoporous silica (SBA-15) was also demonstrated by Zhao et al. [97] in their CO_2 photoreduction studies following 4 h of UV–vis irradiation. They found that an optimal amount of 3% Ce–TiO_2 dispersed on the silica matrix (Ti:Si—1:4) not only facilitated improved textural properties compared to pure TiO_2, but also resulted in an order of magnitude increase in CO (7.5 $\mu mol\,g^{-1}$) and CH_4 (7.9 $\mu mol\,g^{-1}$) production. They reported that the adsorption properties of silica resulting from its unique mesoporous structure was one of the contributing factors due to the increased localized CO_2 concentration near TiO_2 surface where photocatalysis could occur. Clays have been extensively used as supports in photocatalytic studies because of their low-cost and strong absorption capacity [235]. Koci et al. [95] used kaolinite/TiO_2 in CO_2 photoreduction and obtained CH_4 and CH_3OH yields of 4.5 $\mu mol/g_{catal}$ and $\sim$2.5 $\mu mol/g_{catal}$ after 24 h of irradiation. Kaolinite prevented particle aggregation and modified the acid–basic properties of the surface of TiO_2. The use of montmorillonite as support in CO_2 photoreduction has also been examined by Kozak et al. [205]. CH_4, CH_3OH and CO production were observed over ZnS after 24 h of irradiation. Carbon based materials such as graphene/graphene oxide [236–239], carbon nanotubes (CNT) [240] and fullerenes amongst others have attracted wide attention as support materials for TiO_2 induced CO_2 photocatalysis, due to their high specific surface area,

electronic properties and enhanced transport of photogenerated electrons and visible light absorption [241–244]. Recently, hollow spheres consisting of alternating titania ($Ti_{0.91}O_2$) and graphene nanosheets were tested for CO_2 reduction to CO and CH_4 in the presence of water vapor [243]. CH_4 and CO production rates over $Ti_{0.91}O_2$–graphene were 1.14 and 8.91 μmol/g h, respectively, which was reported to be five times higher than $Ti_{0.91}O_2$. Multi walled CNT (MWCNT)/TiO_2 nanocomposites were reported to exhibit superior photocatalytic activity for CO_2 photoreduction compared to anatase TiO_2 and pure MWCNT [244]. Maximum CH_4 yield of 0.178.91 $\mu mol/g_{catal}$ h was achieved after 6 h of visible light irradiation. Thus, the choice of an adequate support is of utmost importance since the overall process efficiency of the photoreactor is predominantly determined by the amount of activated photocatalysts. It is therefore imperative to utilize versatile materials with excellent light transmission properties that can simultaneously serve as catalyst carrier and provide high light transfer area via light distribution from the source to the photocatalyst present within the photoreactor.

5. Support immobilization techniques

TiO_2 based catalysts can be deposited on structured substrates through aqueous or gaseous routes. Some examples of aqueous methods include sol–gel and electrophoretic deposition, while gas phase methods include spray pyrolysis deposition, chemical vapor deposition and physical vapor deposition. Table 3 highlights the advantages and disadvantages of different methods used for immobilising TiO_2 catalysts [245–247].

5.1. Sol–gel method

Sol–gel technique is amongst the most widely used procedure for preparing TiO_2 photocatalysts. This technique is not only noteworthy for achieving excellent chemical homogeneity but, also deriving unique stable structures at low temperatures as well [30,248–250]. The compositional and microstructural properties of the nano-sized samples can be tailored through the control of the precursor chemistry and processing conditions. Inorganic metal salts like titanyl sulphate, titanium tetrachloride etc., (non-alkoxide) and metal alkoxides e.g., titanium(IV) butoxide are usually employed as chemical precursors. Conversion from the liquid sol phase into the solid gel phase occurs due to solvent loss and complete polymerization. The pH of the reaction medium, water:alkoxide ratio and reaction temperatures are factors that influence the sol–gel procedure [251]. Watson et al. [64] demonstrated the preparation of more uniform and pure photocatalysts via the alkoxide route, while Sivakumar et al. [252] used ammonium nitrate and titanyl sulphate as precursors. The rapid hydrolysis rate of titanium alkoxide has been reported as a major drawback that makes this process difficult to control [253]. The sol–gel process is initiated via hydrolysis and polycondensation of metal precursors (Eqs. (21)–(25)) where R stands for C_4H_9 [254,255].

Apart from esterification, the hydrolysing water can also be introduced and controlled through oxolation, as shown in Eq. (22). During condensation, the crystal of the metal oxide can be formed when the constituent particles of the gel are pulled into a compact mass. Additionally, acetic acid modifies and stabilizes the hydrolysis process by altering the alkoxide precursor at molecular level and acting as a chelating ligand, such that Ti—OH bonds were formed when the bidental ligand was broken off (Eq. (25)). The decrease in the hydrolysis rate results in the formation of fine particles of titania which are uniformly dispersed in solution. Appropriate amount of metal precursor(s) can also be introduced within the hydrolysis and polycondensation phase depending on the weight percent loading calculated from the amount of precursors used in the procedure. Sols are usually deposited on the substrates via dip-coating, spin coating, doctor blade techniques amongst others. The withdrawal speed of the substrate, number of coating cycles and the sol viscosity determines the catalyst film thickness. TiO_2 was immobilized onto gas separation membrane by sol–gel dip coating method to study the CO_2 reduction performance [256]. The gas separation membranes were dipped into TiO_2 sol with different withdrawal speeds. Maximum CO production yield of >250 ppm V was observed over the TiO_2 film coated with the withdrawal speed of 0.66 mm/s after 72 h of UV irradiation. The improved activity using this optimum coating condition was attributed to TiO_2 films being thin and even. The synthesized nano-sized TiO_2 films have been to have special catalytic properties due to the integration of the active metal during the gelation stage.

■ Esterification:

$$ROH + CH_3COOH\ H_2O + RCOOC_2H_5 \quad (21)$$

■ Oxolation:

$$Ti(OR)_3\ (OH) + Ti(OR)_3\ (OH) \rightarrow (RO)_3\ Ti{-}O{-}Ti(OR)_3 + H_2O \quad (22)$$

Table 3
Advantages and disadvantages of different methods used for immobilizing TiO_2 photocatalysts.

Catalyst preparation method	Advantages	Disadvantages	References
Sol–gel	High purity of materials Homogeneity Versatile means of processing and control of parameters Large surface area Chemical bonding results in strong adherence of coating to the substrate	Hydrolysis rate is difficult to control Longer processing time compared to CVD and PVD Calcination at high temperatures results in the decomposition of substrates Multiple coating cycles is required depending on the sol viscosity	[248–251]
Physical vapor deposition	Does not require complex chemical reactions Low to medium deposition temperature	Expensive as vacuum systems are used Difficulty in deposition of multiple source precursors due to various evaporation times	[19,245]
Chemical vapor deposition	Suitable for uniform and pure films with high deposition rate Short processing time	Could be expensive if vacuum systems are used Difficulty in deposition of multiple source precursors due to various evaporation times High deposition temperature (>600 °C) is required	[245–247]

■ Hydrolysis:

$$Ti(OR)_4 + H_2O \rightarrow Ti(OR)_3\,(OH) + ROH \quad (23)$$

■ Condensation dehydration:

$$Ti(OR)_3\,(OH) + Ti(OR)_4 \rightarrow (RO)_3\,Ti{-}O{-}Ti(OR)_3 + ROH \quad (24)$$

■ Chelation:

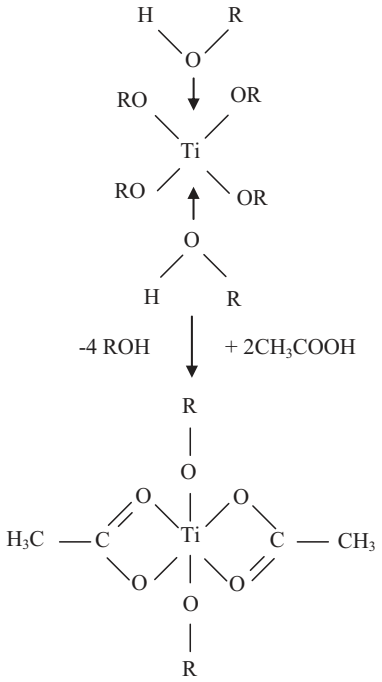

(25)

The series of Cr doped TiO_2 samples synthesized by the sol–gel method was found to promote the CO_2 reforming performance of TiO_2. Under their experimental conditions, the Cr-doped samples showed improved photoresponse in the visible light in their study compared to the pure TiO_2 film. Optimum product yields of 92.5 mmol/g_{catal} (CO), 15.1 mmol/g_{catal} (CH_4) and 19.1 mmol/g_{catal} (C_2H_6) were obtained using the 7 wt% sample. Copper supported on unstructured and inverse opal titania (templates of polystyrene spheres) films coated onto optical fibers by sol–gel dip-coating technique were employed for the photoreduction of gaseous CO_2 to CH_3OH in the presence of water vapor and UV light [157]. Although the methanol production rates of the Cu films supported on inverse opal titania (0.0364 μmol/g_{catal} h) were comparable to the films supported on unstructured titania, much higher quantum efficiency was achieved using the inverse opal film due to improved photon utilization rate observed at a lower light intensity.

5.1.1. Thermal treatment

Calcination is one of the means by which crystal growth can be controlled. The crystal growth influences the phase, shape, size and surface area of photocatalysts. Sol–gel derived precipitates tend to be amorphous in nature and require heat treatment to remove organic molecules from the final products and induce crystallization [251,255]. Amorphous TiO_2 can be converted to anatase phase due to pore collapse and crystal growth of the TiO_2 powder during calcination. With increasing temperatures, calcinations may result in phase transformation, reduced surface area, grain growth and particle aggregation, which affects the microstructure and textural properties (crystallinity, surface area, morphology) of TiO_2 [41,255]. The removal of organics has been reported to occur at temperatures ≥ 673 K [254]. Conversely, well crystallized anatase TiO_2 films can be synthesized by the peptization of tetraisopropyl orthotitanate in acidic conditions at low temperatures [257].

Since photoconversion can only occur when the photogenerated holes and electrons are present on TiO_2 surface, the surface phase of TiO_2 exposed to reactant and light has been found to play a critical role in determining the rate of photoconversion by several researchers [62,75,258]. Consequently, a reasonable calcination temperature must be selected such that increased crystallinity is achieved with the surface area remaining intact and unchanged. Su et al. [255], Vijayan et al. [259] and Schulte et al. [260] demonstrated that their optimum activities were strongly dependent on the crystallinity of their nanostructures. Su et al. [255] showed that optimal photocatalytic activity for decomposition of salicylic acid can be achieved with the sample calcined at 773 K. The photoactivity decrease was observed beyond this temperature due to reduced surface area and decreasing anatase fraction. The anatase to rutile fraction was found to decrease with increasing temperatures.

Conversely, Vijayan et al. [259] observed increased methane production using titania nanotubes calcined between 473–673 K for CO_2 reduction owing to the combined effects of crystallinity and surface area. Declined activity was observed on further temperature increase. The anatase content was also found to play a critical role in the UV activation of nanotubes prepared by Schulte et al. [260] for CO_2 reduction. They also observed declined reactivity with increasing calcination temperature. Increased rutile content at near 953 K was found to tune the photoresponse toward the visible light region which further optimized reactivity of the samples. Amongst the crystalline phases of titania that can be formed during calcination, anatase has been reported to possess better photocatalytic activity for CO_2 reduction compared to rutile due to higher surface areas and improved hole trapping arising from steeper band bending [251]. Phase transformation from anatase to stable rutile can occur upon thermal treatment between temperatures of 623–1373 K owing to different processing methods, precursors and techniques of determining this transition temperature [143,261]. The presence of mixed crystalline phases of titania (i.e., anatase and rutile) has also been reported to show improved photocatalytic activity due to synergistic effect derived from better charge separation and high surface area [262]. Improved charge separation and high reactivity at the anatase to rutile interface occurs during electron transfer from rutile to anatase at this interface where defect sites with unique charge trapping and adsorption properties can be created [62,262,263].

Zhang et al. [258] further investigated the relationship between the effect of calcination temperature and time on the surface phases and photocatalytic activities of TiO_2. The transformation from anatase bulk phase to rutile occurred at 823 K, with the anatase phase still being maintained on the surface till 680 °C. Further temperature increase to ≥973 K led to the complete conversion of the bulk anatase phase into rutile, with only 44% of the anatase phase being present on the TiO_2 surface. Maximum hydrogen production was observed for samples calcined between 973–1023 K due to catalyst's surface consisting of a mixed phase of anatase and rutile particle, with the bulk consisting of almost pure rutile. Similar results were also observed for the samples calcined at 873 K for different time periods between 20 and 80 h. These results were due to the formation of the surface-phase junction which was found to promote electron transfer from the conduction band of rutile to the trapping sites of anatase. Cybula et al. [234] synthesized titania nanoparticles using TiO_2 P25 and found the rate of CO_2 photoreduction to methane was much higher on

temperature increase from 353 to 393 K and drying times from 5 to 20 h. A marked decrease in photoreduction efficiency was observed on further temperature increase to 433 K and drying time of 35 h. Asi et al. [75] synthesized AgBr doped TiO_2 that exhibited good crystallinity and optimal hydrocarbon production rate for the photoreduction of CO_2 under visible light at calcination temperature of 773 K and doping concentration of 23.2 wt%. They found that increasing the calcination temperature to 973 K resulted in the aggregation of the doped nanoparticles which explained the decreased in hydrocarbon production rate.

5.1.2. Influence of organic contaminants

Organic impurities originating from chemical precursors used during catalyst synthesis have been reported to influence the activity and selectivity of CO_2 photoreduction. These organic compounds in the form of carbon and chlorine species which adsorb on the surface of TiO_2 can serve as a carbon or chlorine source for the formation of hydrocarbons or undesired products such as CH_3Cl. By using a combination of in situ diffuse reflectance infrared Fourier transform spectroscopy (DRIFTS) with isotope labelled $^{13}CO_2$, Yang et al. [264] demonstrated that carbon residues present on the catalyst surface were involved in the photocatalytic reduction of CO_2 to CO. It was observed that prolonged exposure of the catalyst surface to UV irradiation and H_2O vapor was more effective for removal of these carbon residues which originated from Ti alkoxides and polyethylene glycol (PEG) than thermal treatment in air. Since adsorbed ^{12}CO species were observed as the main product compared to ^{13}CO over $Cu(I)/TiO_2$ in the absence of $^{12}CO_2$, it was concluded that ^{12}C originating from carbon residues was the predominant carbon source. Isotopic labelling results of Ag, Au and Pd–TiO_2 samples tested for CO_2 reduction also confirmed that CH_4 was formed from organic impurities rather than $^{13}CO_2$ [265]. The formation of chloromethane (CH_3Cl) as a result of CO_2 photoreduction with Cu/I–TiO_2 synthesized from a chlorinated precursor ($CuCl_2$) was observed [181]. CH_3Cl was formed from the reaction of methyl radical ($CH_3^{\bullet}$) with chlorine radical ($Cl^{\cdot}$). Adsorbed carbon species were reported to be intermediates for CH_4 and CH_3Cl formation.

Several authors have employed different spectroscopic techniques such as DRIFTS, GC–MS, NMR or LC–MS with isotope labelled $^{13}CO_2$ as the reactant for verifying the carbon source of final products generated from photocatalytic CO_2 reduction. For example, Yui et al. [266] observed that CO_2 and CO_3^{2-} were the main carbon sources of CH_4 produced using Pd–TiO_2 treated by calcination and washing procedures. Signal of $m/z = 17$ attributed to $^{13}CH_4$ detected by the GC–MS when $^{13}CO_2$ was used as a reactant clearly demonstrated that CH_4 formation was from CO_2 photoreduction and not from residual carbon species. To verify the source of evolved CO and O_2 from CO_2 photoreduction with H_2O, Teramura et al. performed labelling experiments with $^{13}CO_2$ and $H_2{}^{18}O$ as reactants using GC–MS [267]. After photo irradiation, peaks of $^{16}O^{18}O$ and ^{13}CO were detected. The effect of several solvents on CO_2 photoreduction with Q-TiO_2/SiO_2 films was also studied by using ^{13}C NMR and $^{13}CO_2$ to identify the carbon source for CO and C_1–C_2 oxygenates [268]. Labelling experiments confirmed formate and CO were produced from CO_2 and not from the solvents (CCl_4, 2-propanol and acetonitrile). Fu et al. used isotopic $^{13}CO_2$ for the photocatalytic reduction of CO_2 over titanium metal organic framework (MOF) catalysts where obtained products were identified by ^{13}C NMR spectroscopy [269]. Isotopic $^{13}CO_2$ reaction confirmed that the reduced product, $HCOO^-$ originated from CO_2 rather than residual carbon species. Ohno et al. also demonstrated that that CO_2 was the carbon source for CH_3OH evolution with ^1H NMR spectroscopy over Au–TiO_2 (brookite) nanorods and hybrid photocatalyst composed of WO_3 and graphitic carbon nitride [270,271]. In summary, these findings clearly indicate that the choice of catalyst precursors must be carefully considered during catalyst synthesis with systematically designed control experiment [226,266,272] or carbon source verification by GC–MS, NMR or LC–MS with isotope labelled $^{13}CO_2$ in place.

5.2. Vapor deposition

Chemical vapor deposition (CVD) has been widely used in surface coating in CO_2 photoreduction and is prepared via the vapor phase, while the formation of films in physical vapor deposition (PVD) occurs when no chemical reaction takes place. Silija et al. [273] described CVD as a better technique when compared to PVD because better durability, adhesion and uniformity can be achieved with this technique compared to the latter. The need for aging, drying and reduction is also eliminated with CVD. Extensive studies conducted by Choy [245] detailed several variants of CVD and noted the complexity of chemical process as a major difference between CVD and physical vapor deposition (PVD) due to the chemical precursors and reactions used. The kind of precursor and substrate used with the desired properties serves as a determining factor for the type of variant used. The thermal and chemical stability of the support and operating conditions of the volatile precursors i.e., temperature required for crystallization must be carefully considered. Thin films are usually formed in CVD when the surface of the substrate is exposed to volatile precursor(s) in inert atmosphere under controlled temperature and pressure. Nishida et al. [274] demonstrated the use of plasma enhanced CVD for the preparation of thin films of TiO_2 while Galindo et al. [246] reported the use of pulsed injected metal organic CVD technique toward the deposition of multilayer thin films.

Wang et al. [213] synthesized platinized TiO_2 films via the aerosol chemical vapor deposition (ACVD) technique. The synthesized films which have unique one-dimensional structure of TiO_2 single crystals coated with Pt nanoparticles were reported to exhibit high photoefficiency for CO_2 reduction with water vapor following 4 h of UV irradiation. Maximum CH_4 yield of 1361 $\mu mol/g_{catal}\,h^{-1}$ was exhibited by the Pt film with deposition time of 20 s. Overall, high surface area, single crystallinity of the one dimensional TiO_2 films and efficient hole separation were the main reasons described by the authors for the enhanced photoactivity of the films compared to TiO_2. Asi et al. [75] demonstrated the visible light reduction of CO_2 to fuels using AgBr/CNT nanocomposites. Multi-walled carbon nanotubes (CNT) were synthesized by CVD while AgBr was introduced to the CNT framework via deposition–precipitation method in the presence of cation surfactant. Higher product yields were obtained over AgBr/CNT nanocomposites compared to AgBr crystals. The product yield also increased with increasing nanotube length due to efficient charge transport demonstrated by longer nanotubes which was confirmed by electrochemical impedance spectroscopy measurements.

6. Photoreactor design and configuration

The configuration of catalyst particles in a photoreactor system is also another important factor that can influence the overall photocatalytic efficiency [27,28]. Photoreactors are vessels where reaction products are generated from the contact between photocatalysts, reactants and photons. The two key parameters which determine the types of photoreactors utilized in CO_2 photoreduction are the phases involved (i.e., multiphase (gas–solid, liquid–solid, gas–liquid–solid etc.) and the mode of operation (i.e., batch, semi-batch or continuous) [158].

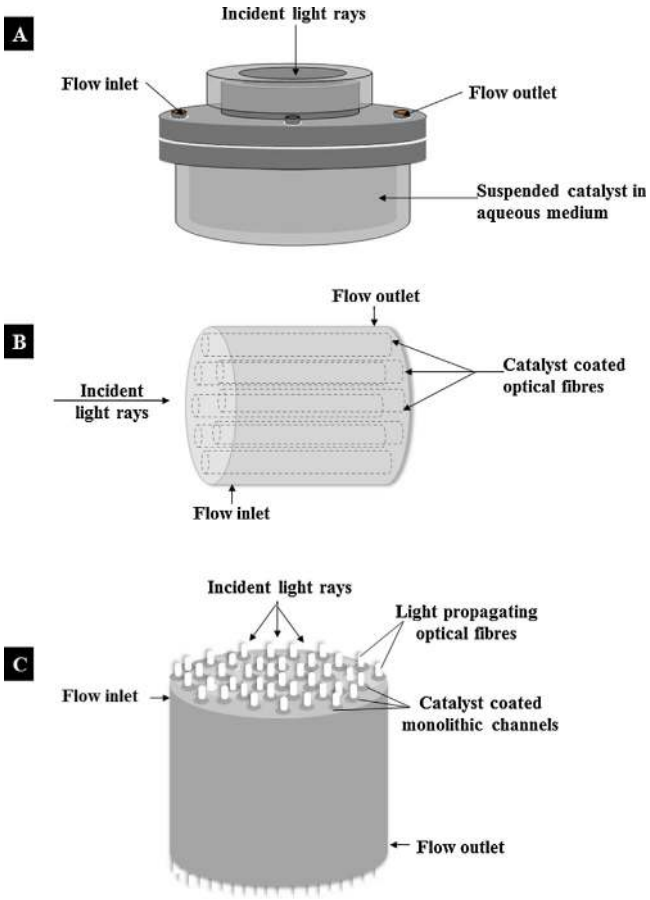

Fig. 10. Schematic of (A) slurry reactor design with top illumination, (B) optical fiber reactor design with side illumination and (C) internally illuminated reactor with top illumination.

Photocatalysts can be generally tested in either suspended or immobilized forms in reactor configurations, as shown in Fig. 10. An ideal photoreactor must have uniform light distribution throughout the entire system in order to achieve optimum results. Currently, comparative analysis of product yield and reactor configurations in CO_2 reduction is primarily reported in terms of quantum efficiency. The advantages and disadvantages of different types of photoreactor systems currently used in CO_2 photoreduction are summarized in Table 4 [275–279].

6.1. Fluidized and slurry reactor designs

When powders are dispersed/suspended in a liquid medium; the quantum efficiency of the catalyst, absorption properties of both reactants and non-reactants in solution and surface light intensity determines the rate of reaction [28]. Some of the key advantages of slurry system are that there is entire external surface illumination during reaction time if the particle size of the catalyst is small with phase segregation not occurring if the solution is homogeneously mixed [27]. Although slurry system designs offer high catalyst loading and ease of construction; separation of catalyst particles from the reaction mixture is a major drawback [221,279]. The size of the catalyst crystals or aggregates (0.05 μm to a few μm) will determine the nature of separation process required which could be expensive and time consuming [158,279]. However, the penetration depth of UV light into the reaction medium can also be limited by the strong light absorption of organic species and catalyst particles [28,219]. A large proportion of catalyst surface area might be inactive due to low photon energy received, as most of the light irradiation is lost due to absorption by liquid when light approaches the catalyst through the bulk liquid phase [280,281]. Light distribution can be better controlled via external or internal illumination. Hydrocarbon formation (CO, CH_3CHO and CH_3CHO_2) was observed over hybrid catalyst, TiO_2:Rh-LHCII tested in a stirred batch reactor under visible light irradiation [272]. Hybrid catalyst, TiO_2:Rh-LHCII was formulated by attaching light-harvesting complexes (LHCII) extracted from spinach to the surface of Rh-doped TiO_2 (TiO_2:Rh) in order to

Table 4
Advantages and disadvantages of photoreactor systems.

Reactor design	Advantages	Disadvantages	References
Fluidized and slurry reactor (multiphase)	(I) Temperature gradients inside the beds can be reduced through vigorous movements caused by the solid passing through the fluids	(I) Filters (liquid phase) and scrubbers (gas) are needed	[13]
	(II) Heat and mass transfer rates increase considerable due to agitated movement of solid particles	(II) Flooding tends to reduce the effectiveness of the catalyst	
	(III) High catalyst loading	(III) Difficulty of separating the catalyst from the reaction mixture	[219,220]
		(IV) Low light utilization efficiency due to absorption and scattering of the light by the reaction medium	
		V) Restricted processing capacities due to mass transport limitations	
Fixed bed reactor	(I) High surface area (II) Fast reaction time (III) The conversion rate per unit mass of the catalyst is high due to the flow regime close to plug flow (IV) Low operating costs due to low pressure drop	(I) Temperature gradient between gas and solid surface is common	[275,280]
Variants of fixed bed designs			
Monolith reactor	(I) High surface to volume ratio and low pressure drop with high flow rate can be achieved (II) Configuration can be easily modified	(I) Low light efficiency due to opacity of channels of the monolith	[276,277]
Optical fiber reactor	(I) High surface area and light utilization efficiency (II) Efficient processing capacities of the catalyst	(I) Maximum use of the reactor volume is not achieved (II) Heat build-up of fibers can lead to rapid catalyst deactivation	[277,278]

enhance the light absorption and increase yields. The quantum efficiency of 0.0411% was achieved using this configuration.

Slurry reactor design with two separate components for oxygen and hydrocarbon evolution separated by a Nafion membrane was tested by Lee at al. [107] under AM 1.5G irradiation. WO_3 was chosen as the oxidation catalyst while $Pt/CuGaAlO_4$ and $Pt/SrTiO_3$:Rh as reduction catalyst. The dual photocatalyst system containing both reduction and oxidation catalysts demonstrated higher quantum efficiency of 0.0051% compared to the single photocatalyst system with $Pt/CuGaAlO_4$ as reduction catalyst only (0.0019%). Photocatalytic reduction of CO_2 with monoethanolamine (MEA) as reductants to form CH_4 using Ti-MCM-41 mesoporous catalysts was studied and compared to other reductants such as NaOH and H_2O in slurry reactor designs [184]. Photoreduction efficiency of Ti-MCM-41(50) sample 8 h of UV illumination using H_2O, NaOH and MEA as reductants were 0.83, 0.29 and 9.18%, respectively. Copper or cobalt incorporated TiO_2 supported ZSM-5 catalysts were tested in a slurry photoreactor where 0.1 M $NaHCO_3$ was the reductant [282]. When $Cu–TiO_2$/ZSM-5 was used as the catalyst, the quantum efficiency of CH_3OH reached 10.11% after 12 h reaction time. High absorption ability of ZSM-5 was reported to influence the photoconversion rates.

6.2. Fixed bed reactor designs

The drawback of catalyst separation can be avoided by fixed bed reactor designs where catalysts are immobilized onto fixed supports e.g., plate, beads, fibers, monolith etc. In these systems, photocatalysts are coated on a support matrix placed inside the reactor around the light source or directly on the photoreactor wall. Light distribution becomes a limiting factor in this system which is influenced by the geometry of the light source and spatial distance between this light source and photocatalysts [197]. Overall, gas phase systems offer more flexibility compared to the slurry systems if the design considers the spatial relationship between the reactor and the light source when choosing the support of choice. Several researchers have designed photoreactors using optical fibers as supports [217,278,283]. The conventional optical fiber reactor (OFR) has been modified by using fibers with different cores and coatings [218,284], increasing their diameter to create ease of handling and the use of cooling systems [285] to eliminate the limitation of heat build-up. Wu et al. [154,286] have conducted CO_2 photoreduction studies using the optical fiber reactor system. They coated optical fibers with Cu/TiO_2 and Ag/TiO_2 catalysts in the gaseous phase, respectively. A maximum yield of 0.91 $\mu mol/g_{catal}$ h was observed using the loading ratio of 0.5 wt% $Cu–Fe/TiO_2$ for methane production. Maximum methanol yield of 0.45 $\mu mol/g_{catal}$ h was observed by Wu et al. [286] using 1.2 wt% Cu/TiO_2 under light intensity of 16 W/cm^2 while methanol yield of 4.12 $\mu mol/g_{catal}$ h was observed by Wu et al. [154] using 1 wt% Ag/TiO_2 under light intensity of 10 W/cm^2. In particular, previous CO_2 photoreduction studies conducted by Nguyen and Wu [219] using optical fibers coated with $Cu–Fe/TiO_2$ catalysts in the gaseous phase have demonstrated that the number of optical fibers can determine the rate of ethylene production and selectively increase or decrease the quantum yield. A maximum yield of 0.91 $\mu mol/g_{catal}$ h was observed using the loading ratio of 0.5 wt% $Cu–Fe/TiO_2$ for CH_4 production. CO_2 photocatalytic activity of $NiO/InTaO_4$ catalysts dispersed in aqueous solution of NaOH (slurry designs) and immobilized in a fixed bed reactor design containing 216 optical fibers was evaluated by Wang et al. [193]. The quantum efficiency for methanol production was 14 times higher in optical-fiber reactor (0.053%) than that of the aqueous-phase reactor (0.0045%). The higher quantum efficiency was attributed to improved light efficiency by the films coated on optical fibers. The comparison between the photocatalytic reduction of CO_2 for 1 wt% Pd/0.01 wt% $Rh–TiO_2$ in a slurry batch annular reactor system and internally illuminated photoreactor system was evaluated [155]. The quantum efficiency of the internally illuminated monolith reactor (0.049%) was near one order of magnitude higher than the slurry batch annular reactor (0.002%). The performance of TiO_2 for CO production was evaluated in cell type and multichannel monolith reactor [226]. The performance comparison between the gas phase photoreactors revealed 8 fold higher yield of CO in the monolith compared to cell type reactor. Quantum efficiency in microchannel monolith reactor was 0.0301% compared to 0.0028% in the cell type reactor. Improved quantum efficiency was reported to be due to higher illuminated surface area, higher photon energy consumption and better utilization of reactor volume.

7. Conclusions and future perspectives

The utilization of CO_2 as a direct feedstock for photocatalytic conversion into fuels over different variants of pure and modified TiO_2 synthesized by various routes and tested in various photoreactor designs has been highlighted in this review. Application of TiO_2 induced photocatalysis for the challenging conversion of CO_2 remains a promising pathway as it can be activated by solar energy at relatively mild conditions to form valuable products. Although recent progress focused on the use of pure and modified photoactivated TiO_2 materials has induced fuel generation from CO_2 reduction with H_2O; expected improvement required for scalable fuel production has not been achieved. To this end, design and synthesis of novel TiO_2 photocatalysts with higher stability, selectivity and efficiency requires improvements in synthetic procedures offering improved control over physicochemical properties. Analytical techniques such as in-situ surface and bulk spectroscopies must be employed to provide valuable insight into fundamental steps occurring in CO_2 photocatalytic reduction, rate limiting steps, formation and stability of surface reaction intermediates as well as adsorption and desorption of both reactant and product species. Besides the materials science aspect of CO_2 photocatalytic reduction, the engineering challenge of optimal CO_2 photoreactor design needs a step change transformation to reach its crucial role in the overall process performance. From this review, it can be concluded that CO_2 photocatalysis is still not feasible due to the absence of scalable reactor designs able to simultaneously introduce reactants, light and efficient visible light responsive catalysts to effect production of specific fuels in significant quantities. Since the overall process efficiency is largely dependent on two factors—the reactor configuration and physicochemical properties of the catalyst, it is desirable to scale up this system based on the design and development of these parameters incorporating maximal light efficiency and mass transfer. Performance of current photoreactor designs is primarily reported and evaluated in terms of quantum efficiency without consideration of light transport to active site which is critical for scale-up and quantification of energy losses due to light absorption by reaction media and reactor components. A deep understanding of engineering aspects of CO_2 reduction is still required for the development of highly efficient photoreactor designs. In order to achieve high conversion efficiency, photoreactor designs must take into account the material of construction, its thickness, mass of catalyst, reactor geometry (length, volume etc.), flow rate and the relationship between the reactor and irradiation source. The modelling of the effect of reactor designs and operation parameters on CO_2 reduction is also required to extrapolate results for the design of pilot scale systems. Furthermore, this work can be extended to include the use of flue gas generated from power plants as a feedstock for CO_2 reduction. Different compositions of flue gas streams can be used directly or indirectly in order to

ascertain the effect of impurities and the concentration of CO_2 required to achieve maximum conversion rates. Results from using concentrated CO_2 gas streams derived from the flue gas can also be tested and compared to pure flue gas streams to determine the most suitable option for scalable fuel production.

Acknowledgements

The authors thank the financial support provided by the School of Engineering and Physical Sciences and the Centre for Innovation in Carbon Capture and Storage (EPSRC grant number EP/K021796/1) at Heriot-Watt University.

References

[1] IPCC. Special Report on Renewable Energy Sources and Climate Change Mitigation. [cited 2014 November 19]. http://www.ipcc.ch/report/srren/ (2011).
[2] C. Global, The Global Status Of CCS, Institute (GCCSI), Canberra, Australia, 2012.
[3] P. Moriarty, D. Honnery, Mitigating greenhouse: limited time, limited options, Energy Policy 364 (2008) 1251–1256.
[4] J.O.M. Bockris, Would methanol formed from CO_2 from the atmosphere give the advantage of hydrogen at lesser cost? Int. J. Hydrogen Energy 35 (11) (2010) 5165–5172.
[5] C. Song, Global challenges and strategies for control, conversion and utilization of CO_2 for sustainable development involving energy, catalysis, adsorption and chemical processing, Catal. Today 115 (1) (2006) 2–32.
[6] J.A. Turner, A realizable renewable energy future, Science 285 (5428) (1999) 687–689.
[7] M. Grimston, et al., The European and global potential of carbon dioxide sequestration in tackling climate change, Clim. Policy 1 (2) (2001) 155–171.
[8] M. Olivares-Marín, M.M. Maroto-Valer, Development of adsorbents for CO_2 capture from waste materials: a review, Greenhouse Gases Sci. Technol. 2 (1) (2012) 20–35.
[9] S. Bachu, et al., CO_2 storage capacity estimation: methodology and gaps, Int. J. Greenhouse Gas Control 1 (4) (2007) 430–443.
[10] S. Bachu, CO_2 storage in geological media: role, means, status and barriers to deployment, Prog. Energy Combust. Sci. 34 (2) (2008) 254–273.
[11] M. Aresta, A. Dibenedetto, Utilisation of CO_2 as a chemical feedstock: opportunities and challenges, Dalton Trans. 28 (2007) 2975–2992.
[12] K. Koci, L. Obalova, Z. Lacny, Photocatalytic reduction of CO_2 over TiO_2 based catalysts, Chem. Papers 62 (1) (2008) 1–9.
[13] P. Usubharatana, et al., Photocatalytic process for CO_2 emission reduction from industrial flue gas streams, Ind. Eng. Chem. Res. 45 (8) (2006) 2558–2568.
[14] M. Mikkelsen, M. Jorgensen, F.C. Krebs, The teraton challenge. A review of fixation and transformation of carbon dioxide, Energy Environ. Sci. 3 (1) (2010) 43–81.
[15] H. Yano, et al., Efficient electrochemical conversion of CO_2 to CO, C_2H_4 and CH_4 at a three-phase interface on a Cu net electrode in acidic solution, J. Electroanal. Chem. 519 (1–2) (2002) 93–100.
[16] J. Yano, et al., Selective ethylene formation by pulse-mode electrochemical reduction of carbon dioxide using copper and copper-oxide electrodes, J. Solid State Electrochem. 11 (4) (2007) 554–557.
[17] Creutz, F. Fujita, Carbon dioxide as a feedstock, Carbon Management: Implications for R&D in the Chemical Sciences and Technology: A Workshop Report to the Chemical Sciences Roundtable, National Academies Press, Washington, D.C., US, 2001.
[18] M.M. Maroto-Valer, Developments And Innovation In Carbon Dioxide (CO_2) Capture And Storage Technology: Carbon Dioxide (CO_2) Storage And Utilization, Taylor & Francis, 2010, 2015.
[19] O. Carp, C.L. Huisman, A. Reller, Photoinduced reactivity of titanium dioxide, Prog. Solid State Chem. 32 (1–2) (2004) 33–177.
[20] Slamet, et al., Photocatalytic reduction of CO_2 on copper-doped titania catalysts prepared by improved-impregnation method, Catal. Commun. 6 (5) (2005) 313–319.
[21] N. Murakami, et al., Photocatalytic reduction of carbon dioxide over shape-controlled titanium(IV) oxide nanoparticles with co-catalyst loading, Curr. Org. Chem. 17 (21) (2013) 2449–2453.
[22] O. Ishitani, et al., Photocatalytic reduction of carbon dioxide to methane and acetic acid by an aqueous suspension of metal-deposited TiO_2, J. Photochem. Photobiol. A 72 (3) (1993) 269–271.
[23] F. Solymosi, I. Tombacz, Photocatalytic reaction of $H_2O + CO_2$ over pure and doped Rh/TiO_2, Catal. Lett. 27 (1–2) (1994) 61–65.
[24] R. Asahi, et al., Visible-light photocatalysis in nitrogen-doped titanium oxides, Science 293 (5528) (2001) 269–271.
[25] Q. Zhang, et al., Visible light responsive iodine-doped TiO_2 for photocatalytic reduction of CO_2 to fuels, Appl. Catal. A 400 (1–2) (2011) 195–202.
[26] M. Sahu, P. Biswas, Single-step processing of copper-doped titania nanomaterials in a flame aerosol reactor, Nanoscale Res. Lett. 6 (1) (2011) 1–14.
[27] M. Bideau, et al., On the immobilization of titanium dioxide in the photocatalytic oxidation of spent waters, J. Photochem. Photobiol. A 91 (2) (1995) 137–144.
[28] A.K. Ray, A.A. Beenackers, Development of a new photocatalytic reactor for water purification, Catal. Today 40 (1) (1998) 73–83.
[29] Z. Jiang, et al., Turning carbon dioxide into fuel, Philos. Trans. R. Soc. A 368 (1923) (2010) 3343–3364.
[30] U. Akpan, B. Hameed, Parameters affecting the photocatalytic degradation of dyes using TiO_2-based photocatalysts: a review, J. Hazard. Mater. 170 (2) (2009) 520–529.
[31] K. Kočí, L. Obalová, Z. Lacný, Photocatalytic reduction of CO_2 over TiO_2 based catalysts, Chem. Papers 62 (1) (2008) 1–9.
[32] A.L. Linsebigler, G. Lu, J.T. Yates Jr, Photocatalysis on TiO_2 surfaces: principles, mechanisms, and selected results, Chem. Rev. 95 (3) (1995) 735–758.
[33] V.P. Indrakanti, J.D. Kubicki, H.H. Schobert, Photoinduced activation of CO_2 on Ti-based heterogeneous catalysts: current state, chemical physics-based insights and outlook, Energy Environ. Sci. 2 (7) (2009) 745–758.
[34] Marinkovic, et al., Modern Aspects of Electrochemistry, vol. 42, Springer, New York, 2008.
[35] S.N. Habisreutinger, L. Schmidt-Mende, J.K. Stolarczyk, Photocatalytic reduction of CO_2 on TiO_2 and other semiconductors, Angew. Chem. Int. Ed. 52 (29) (2013) 7372–7408.
[36] P.D. Tran, et al., Recent advances in hybrid photocatalysts for solar fuel production, Energy Environ. Sci. 5 (3) (2012) 5902–5918.
[37] K. Wang, et al., Sulfur-doped g-C_3N_4 with enhanced photocatalytic CO_2-reduction performance, Appl. Catal. B 176–177 (2015) 44–52.
[38] B. Wang, H. Yang, T. Xian, L. Di, J.R.S. Li, X.X. Wang, Synthesis of spherical Bi_2WO_6 nanoparticles by a hydrothermal route and their photocatalytic properties, J. Nanomater. (2015) 1–7.
[39] A. Mills, S. Le Hunte, An overview of semiconductor photocatalysis, J. Photochem. Photobiol. A 108 (1) (1997) 1–35.
[40] D. Beydoun, et al., Role of nanoparticles in photocatalysis, J. Nanoparticle Res. 1 (4) (1999) 439–458.
[41] S.M. Gupta, M. Tripathi, A review of TiO_2 nanoparticles, Chin. Sci. Bull. 56 (16) (2011) 1639–1657.
[42] M.A. Fox, M.T. Dulay, Heterogeneous photocatalysis, Chem. Rev. 93 (1) (1993) 341–357.
[43] D.W. Bahnemann, C. Kormann, M.R. Hoffmann, Preparation and characterization of quantum size zinc oxide: a detailed spectroscopic study, J. Phys. Chem. 91 (14) (1987) 3789–3798.
[44] V. Jeyalakshmi, et al., Photocatalytic reduction of carbon dioxide by water: a step towards sustainable fuels and chemicals, Materials Science Forum, Trans Tech Publication, 2013.
[45] U. Diebold, The surface science of titanium dioxide, Surf. Sci. Rep. 48 (5–8) (2003) 53–229.
[46] L. Chen, et al., Photoreduction of CO_2 by TiO_2 nanocomposites synthesized through reactive direct current magnetron sputter deposition, Thin Solid Films 517 (19) (2009) 5641–5645.
[47] Y. Kohno, et al., Photoreduction of CO_2 with H_2 over ZrO_2. A study on interaction of hydrogen with photoexcited CO_2, Phys. Chem. Chem. Phys. 2 (11) (2000) 2635–2639.
[48] T.V. Nguyen, J.C.S. Wu, Photoreduction of CO_2 to fuels under sunlight using optical-fiber reactor, Sol. Energy Mater. Sol. Cells 92 (8) (2008) 864–872.
[49] G. Guan, T. Kida, A. Yoshida, Reduction of carbon dioxide with water under concentrated sunlight using photocatalyst combined with Fe-based catalyst, Appl. Catal. B 41 (4) (2003) 387–396.
[50] S. Qin, et al., Photocatalytic reduction of CO_2 in methanol to methyl formate over CuO–TiO_2 composite catalysts, J. Colloid Interface Sci. 356 (1) (2011) 257–261.
[51] L. Jia, J. Li, W. Fang, Enhanced visible-light active C and Fe co-doped $LaCoO_3$ for reduction of carbon dioxide, Catal. Commun. 11 (2) (2009) 87–90.
[52] K. Teramura, et al., Effect of H_2 gas as a reductant on photoreduction of CO_2 over a Ga_2O_3 photocatalyst, Chem. Phys. Lett. 467 (1–3) (2008) 191–194.
[53] K. Teramura, et al., Photocatalytic reduction of CO_2 using H_2 as reductant over $ATaO_3$ photocatalysts (A = Li, Na, K), App. Catal. B 96 (3–4) (2010) 565–568.
[54] J.C. Colmenares, et al., Nanostructured photocatalysts and their applications in the photocatalytic transformation of lignocellulosic biomass: an overview, Materials 2 (4) (2009) 2228–2258.
[55] M. Bellardita, et al., Photocatalytic behaviour of metal-loaded TiO_2 aqueous dispersions and films, Chem. Phys. 339 (1–3) (2007) 94–103.
[56] S. Malato, et al., Decontamination and disinfection of water by solar photocatalysis: recent overview and trends, Catal. Today 147 (1) (2009) 1–59.
[57] L. Yuan, Y.-J. Xu, Photocatalytic conversion of CO_2 into value-added and renewable fuels, Appl. Surf. Sci. 342 (2015) 154–167.
[58] M. Marszewski, S. Cao, J. Yu, M. Jaroniec, Semiconductor-based photocatalytic CO_2 conversion, Mater. Horizons 2 (3) (2015) 261–278.
[59] X. Li, et al., Design and fabrication of semiconductor photocatalyst for photocatalytic reduction of CO_2 to solar fuel, Sci. China Mater. 57 (1) (2014) 70–100.
[60] V.P. Indrakanti, Kubicki, H.H. Schobert, Photoinduced activation of CO_2 on Ti-based heterogeneous catalysts: current state, chemical physics-based insights and outlook, Energy Environ. Sci. 2 (7) (2009) 745–758.

[61] G. Li Puma, et al., Preparation of titanium dioxide photocatalyst loaded onto activated carbon support using chemical vapor deposition: a review paper, J. Hazard. Mater. 157 (2–3) (2008) 209–219.
[62] P. Bouras, E. Stathatos, P. Lianos, Pure versus metal-ion-doped nanocrystalline titania for photocatalysis, Appl. Catal. B 73 (1–2) (2007) 51–59.
[63] W.A. Zeltner, D.T. Tompkins, L. Harriman, Shedding light on photocatalysis. Discussion, ASHRAE Trans. (2005) 523–534.
[64] S. Watson, et al., Preparation of nanosized crystalline TiO_2 particles at low temperature for photocatalysis, J. Nanoparticle Res. 6 (2) (2004) 193–207.
[65] A. Fujishima, X. Zhang, D.A. Tryk, TiO_2 photocatalysis and related surface phenomena, Surf. Sci. Rep. 63 (12) (2008) 515–582.
[66] M. Kitano, et al., Recent developments in titanium oxide-based photocatalysts, Appl. Catal. A 325 (1) (2007) 1–14.
[67] F. Han, et al., Tailored titanium dioxide photocatalysts for the degradation of organic dyes in wastewater treatment: a review, Appl. Catal. A 359 (1) (2009) 25–40.
[68] O. Ola, M.M. Maroto-Valer, Transition metal oxide based TiO_2 nanoparticles for visible light induced CO_2 photoreduction, Appl. Catal. A 502 (2015) 114–121.
[69] X. Chen, Titanium dioxide nanomaterials: synthesis, properties, modifications, and applications, Cheminform 38 (41) (2007) .
[70] O. Ozcan, et al., Dye sensitized artificial photosynthesis in the gas phase over thin and thick TiO_2 films under UV and visible light irradiation, Appl. Catal. B Environ. 71 (3–4) (2007) 291–297.
[71] T.-V. Nguyen, J.C.S. Wu, C.-H. Chiou, Photoreduction of CO_2 over ruthenium dye-sensitized TiO_2-based catalysts under concentrated natural sunlight, Catal. Commun. 9 (10) (2008) 2073–2076.
[72] K.R. Thampi, J. Kiwi, M. Graetzel, Methanation and photo-methanation of carbon dioxide at room temperature and atmospheric pressure, Nature 327 (6122) (1987) 506–508.
[73] G. Qin, et al., Photocatalytic reduction of carbon dioxide to formic acid, formaldehyde, and methanol using dye-sensitized TiO_2 film, Appl. Catal. B 129 (2013) 599–605.
[74] C.J. Wang, et al., Visible light photoreduction of CO_2 using CdSe/Pt/TiO_2 heterostructured catalysts, J. Phys. Chem. Lett. 1 (1) (2010) 48–53.
[75] M. Abou Asi, et al., Photocatalytic reduction of CO_2 to hydrocarbons using AgBr/TiO_2 nanocomposites under visible light, Catal. Today 175 (1) (2011) 256–263.
[76] C. Wang, et al., Size-dependent photocatalytic reduction of CO_2 with PbS quantum dot sensitized TiO_2 heterostructured photocatalysts, J. Mater. Chem. 21 (35) (2011) 13452–13457.
[77] X. Li, et al., Adsorption of CO_2 on heterostructure CdS (Bi_2S_3)/TiO_2 nanotube photocatalysts and their photocatalytic activities in the reduction of CO_2 to methanol under visible light irradiation, Chem. Eng. J. 180 (2012) 151–158.
[78] Y. Wang, et al., Ordered mesoporous CeO_2–TiO_2 composites: highly efficient photocatalysts for the reduction of CO_2 with H_2O under simulated solar irradiation, Appl. Catal. B 130 (2013) 277–284.
[79] A.A. Beigi, S. Fatemi, Z. Salehi, Synthesis of nanocomposite CdS/TiO_2 and investigation of its photocatalytic activity for CO_2 reduction to CO and CH_4 under visible light irradiation, J. CO_2 Util. 7 (2014) 23–29.
[80] K. Kočí, et al., Sol–gel derived Pd supported TiO_2–ZrO_2 and TiO_2 photocatalysts; their examination in photocatalytic reduction of carbon dioxide, Catal. Today 230 (2014) 20–26.
[81] G. Marcì, E.I. García-López, L. Palmisano, Photocatalytic CO_2 reduction in gas–solid regime in the presence of H_2O by using GaP/TiO_2 composite as photocatalyst under simulated solar light, Catal. Commun. 53 (2014) 38–41.
[82] N. Sasirekha, S.J.S. Basha, K. Shanthi, Photocatalytic performance of Ru doped anatase mounted on silica for reduction of carbon dioxide, Appl. Catal. B 62 (1–2) (2006) 169–180.
[83] S.S. Tan, L. Zou, E. Hu, Photosynthesis of hydrogen and methane as key components for clean energy system, Sci. Technol. Adv. Mater. 8 (1) (2007) 89–92.
[84] J.C.S. Wu, et al., Application of optical-fiber photoreactor for CO_2 photocatalytic reduction, Top. Catal. 47 (3–4) (2008) 131–136.
[85] J. Wu, Photocatalytic reduction of greenhouse gas CO_2 to fuel, Catal. Surv. Asia 13 (1) (2009) 30–40.
[86] H.W.N. Slamet, et al., Effect of copper species in a photocatalytic synthesis of methanol from carbon dioxide over copper-doped titania catalysts, World Appl. Sci. J. 6 (1) (2009) 112–122.
[87] I.H. Tseng, W.C. Chang, J.C.S. Wu, Photoreduction of CO_2 using sol–gel derived titania and titania-supported copper catalysts, Appl. Catal. B 37 (1) (2002) 37–48.
[88] I.H. Tseng, J.C.S. Wu, H.Y. Chou, Effects of sol–gel procedures on the photocatalysis of Cu/TiO_2 in CO_2 photoreduction, J. Catal. 221 (2) (2004) 432–440.
[89] S.S. Tan, L. Zou, E. Hu, Photocatalytic reduction of carbon dioxide into gaseous hydrocarbon using TiO_2 pellets, Catal. Today 115 (1–4) (2006) 269–273.
[90] S. Krejčíková, et al., Preparation and characterization of Ag-doped crystalline titania for photocatalysis applications, Appl. Catal. B 111 (2012) 119–125.
[91] Q.-H. Zhang, et al., Photocatalytic reduction of CO_2 with H_2O on Pt-loaded TiO_2 catalyst, Catal. Today 148 (3–4) (2009) 335–340.
[92] T.-f. Xie, et al., Application of surface photovoltage technique in photocatalysis studies on modified TiO_2 photo-catalysts for photo-reduction of CO_2, Mater. Chem. Phys. 70 (1) (2001) 103–106.
[93] H.C. Yang, et al., Mesoporous TiO_2/SBA-15, and Cu/TiO_2/SBA-15 composite photocatalysts for photoreduction of CO_2 to methanol, Catal. Lett. 131 (3–4) (2009) 381–387.
[94] Y. Li, et al., Photocatalytic reduction of CO_2 with H_2O on mesoporous silica supported Cu/TiO_2 catalysts, Appl. Catal. B 100 (1–2) (2010) 386–392.
[95] K. Kocí, et al., Comparison of the pure TiO_2 and kaolinite/TiO_2 composite as catalyst for CO_2 photocatalytic reduction, Catal. Today 161 (1) (2011) 105–109.
[96] J. Wei, et al., Characterization of Y/TiO_2 nanoparticles and their reactivity for CO_2 photoreduction, Appl. Mech. Mater. 55 (2011) 1506–1510.
[97] C. Zhao, et al., Photocatalytic conversion of CO_2 and H_2O to fuels by nanostructured Ce–TiO_2/SBA-15 composites, Catal. Sci. Technol. 2 (12) (2012) 2558–2568.
[98] L. Collado, et al., Enhancement of hydrocarbon production via artificial photosynthesis due to synergetic effect of Ag supported on TiO_2 and ZnO semiconductors, Chem. Eng. J. 224 (2013) 128–135.
[99] B.S. Kwak, et al., Methane formation from photoreduction of CO_2 with water using TiO_2 including Ni ingredient, Fuel 143 (2015) 570–576.
[100] Y. Liu, et al., Photocatalytic reduction of CO_2 with water vapor on surface La-modified TiO_2 nanoparticles with enhanced CH_4 selectivity, Appl. Catal. B 168–169 (2015) 125–131.
[101] C. Tang, et al., CeF_3/TiO_2 composite as a novel visible-light-driven photocatalyst based on upconversion emission and its application for photocatalytic reduction of CO_2, J. Lumin. 154 (2014) 305–309.
[102] O. Ola, M. Mercedes Maroto-Valer, Role of catalyst carriers in CO_2 photoreduction over nanocrystalline nickel loaded TiO_2-based photocatalysts, J. Catal. 309 (2014) 300–308.
[103] S. Rani, N. Bao, S.C. Roy, Solar spectrum photocatalytic conversion of CO_2 and water vapor into hydrocarbons using TiO_2 nanoparticle membranes, Appl. Surf. Sci. 289 (2014) 203–208.
[104] L. Matejova, et al., Preparation, characterization and photocatalytic properties of cerium doped TiO_2: on the effect of Ce loading on the photocatalytic reduction of carbon dioxide, Appl. Catal. B 152 (153) (2014) 172–183.
[105] Y. Wang, et al., High efficiency photocatalytic conversion of CO_2 with H_2O over Pt/TiO_2 nanoparticles, RSC Adv. 4 (84) (2014) 44442–44451.
[106] P. Akhter, et al., New nanostructured silica incorporated with isolated Ti material for the photocatalytic conversion of CO_2 to fuels, Nanoscale Res. Lett. 9 (1) (2014) 1–8.
[107] W.-H. Lee, et al., A novel twin reactor for CO_2 photoreduction to mimic artificial photosynthesis, Appl. Catal. B 132 (2013) 445–451.
[108] Y.-H. Cheng, et al., Photo-enhanced hydrogenation of CO_2 to mimic photosynthesis by CO co-feed in a novel twin reactor, Appl. Energy 147 (2015) 318–324.
[109] F. Saladin, L. Forss, I. Kamber, Photosynthesis of CH_4 at a TiO_2 surface from gaseous H_2O and CO_2, J. Chem. Soc. Chem. Commun. 5 (1995) 533–534.
[110] K. Iizuka, et al., Photocatalytic reduction of carbon dioxide over Ag cocatalyst-loaded $ALa_4Ti_4O_{15}$ (A = Ca, Sr, and Ba) using water as a reducing reagent, J. Am. Chem. Soc. 133 (51) (2011) 20863–20868.
[111] K. Ogura, et al., Visible-light-assisted decomposition of H_2O and photomethanation of CO_2 over CeO_2–TiO_2 catalyst, J. Photochem. Photobiol. A 66 (1) (1992) 91–97.
[112] Q. Li, et al., Photocatalytic reduction of CO_2 on MgO/TiO_2 nanotube films, Appl. Surf. Sci. 314 (2014) 458–463.
[113] M. Tahir, N.S. Amin, Indium-doped TiO_2 nanoparticles for photocatalytic CO_2 reduction with H_2O vapors to CH_4, Appl. Catal. B 162 (2015) 98–109.
[114] M. Hussain, et al., Nanostructured TiO_2/KIT-6 catalysts for improved photocatalytic reduction of CO_2 to tunable energy products, Appl. Catal. B 170–171 (2015) 53–65.
[115] J. Fan, et al., Synergistic effect of N and Ni^{2+} on nanotitania in photocatalytic reduction of CO_2, J. Environ. Eng. 137 (3) (2010) 171–176.
[116] O.K. Varghese, et al., High-rate solar photocatalytic conversion of CO_2 and water vapor to hydrocarbon fuels, Nano Lett. 9 (2) (2009) 731–737.
[117] Z. Zhao, et al., Effect of heating temperature on photocatalytic reduction of CO_2 by N–TiO_2 nanotube catalyst, Catal. Commun. 21 (2012) 32–37.
[118] L.M. Xue, et al., Preparation of C doped TiO_2 photocatalysts and their photocatalytic reduction of carbon dioxide, Adv. Mater. Res. 183 (2011) 1842–1846.
[119] B. Michalkiewicz, et al., Reduction of CO_2 by adsorption and reaction on surface of TiO_2-nitrogen modified photocatalyst, J. CO_2 Util. 5 (2014) 47–52.
[120] S. Zhou, et al., Facile in situ synthesis of graphitic carbon nitride (g-C_3N_4)–N–TiO_2 heterojunction as an efficient photocatalyst for the selective photoreduction of CO_2 to CO, Appl. Catal. B 158–159 (2014) 20–29.
[121] T. Phongamwong, M. Chareonpanich, J. Limtrakul, Role of chlorophyll in spirulina on photocatalytic activity of CO_2 reduction under visible light over modified N-doped TiO_2 photocatalysts, Appl. Catal. B 168–169 (2015) 114–124.
[122] M. Ni, et al., A review and recent developments in photocatalytic water-splitting using TiO_2 for hydrogen production, Renew. Sustain. Energy Rev. 11 (3) (2007) 401–425.
[123] K. Kalyanasundaram, M. Graetzel, Artificial photosynthesis: biomimetic approaches to solar energy conversion and storage, Curr. Opin. Biotechnol. 21 (3) (2010) 298–310.
[124] Y. Cho, et al., Visible light-induced degradation of carbon tetrachloride on dye-sensitized TiO_2, Environ. Sci. Technol. 35 (5) (2001) 966–970.

[125] H. Ross, J. Bendig, S. Hecht, Sensitized photocatalytical oxidation of terbutylazine, Sol. Energy Mater. Sol. Cells 33 (4) (1994) 475–481.
[126] G. Mele, et al., Photocatalytic degradation of 4-nitrophenol in aqueous suspension by using polycrystalline TiO_2 samples impregnated with Cu(II)-phthalocyanine, Appl. Catal. B 38 (4) (2002) 309–319.
[127] M. Grätzel, Perspectives for dye-sensitized nanocrystalline solar cells, Prog. Photovoltaics Res. Appl. 8 (1) (2000) 171–185.
[128] S.G. Kumar, L.G. Devi, Review on modified TiO_2 photocatalysis under UV/visible light: selected results and related mechanisms on interfacial charge carrier transfer dynamics, J. Phys. Chem. A 115 (46) (2011) 13211–13241.
[129] Y.-J. Yuan, et al., A copper(i) dye-sensitised TiO_2-based system for efficient light harvesting and photoconversion of CO_2 into hydrocarbon fuel, Dalton Trans. 41 (32) (2012) 9594–9597.
[130] M. Anpo, Preparation, characterization, and reactivities of highly functional titanium oxide-based photocatalysts able to operate under UV–visible light irradiation: approaches in realizing high efficiency in the use of visible light, Bull. Chem. Soc. Jpn. 77 (8) (2004) 1427–1442.
[131] C. Comninellis, G. Chen, Electrochemistry for the Environment, Springer, 2010, 2015.
[132] H. Shon, et al., Visible light responsive titanium dioxide (TiO_2), J. Korean Ind. Eng. Chem. 19 (1) (2008) 1–16.
[133] Y. Ma, et al., Titanium dioxide-based nanomaterials for photocatalytic fuel generations, Chem. Rev. 114 (19) (2014) 9987–10043.
[134] W. Sigmund, H. El-Shall, O. Dinesh Shah, M. Brij Moudgil, Particulate Systems in Nano- and Biotechnologies, CRC Press, Boca Raton, 2008.
[135] H. Fujii, et al., Preparation and photocatalytic activities of a semiconductor composite of CdS embedded in a TiO_2 gel as a stable oxide semiconducting matrix, J. Mol. Catal. A: Chem. 129 (1) (1998) 61–68.
[136] H.C. Liang, X.Z. Li, J. Nowotny, Photocatalytical properties of TiO_2 nanotubes, Solid State Phenom. 162 (2010) 295–328.
[137] G. Liu, et al., Titania-based photocatalysts–crystal growth, doping and heterostructuring, J. Mater. Chem. 20 (5) (2010) 831–843.
[138] D.A. Neamen, Semiconductor Physics and Devices: Basic Principles, McGraw Hill, Singapore, 2012.
[139] M.F. Ashby, R.W. Messler, R. Asthana, E.P. Furlani, R.E. Smallman, A.H.W. Ngan, R.J. Crawford, N. Mills, Engineering Materials and Processes Desk Reference, Oxford, Butterworth-Heinemann, 2009.
[140] B.D. Fahlman, Materials Chemistry, Springer, Netherlands, 2008.
[141] B. Pajot, B. Clerjaud, Optical Absorption of Impurities and Defects in Semiconducting Crystals, vol. 169, Springer, Netherlands, 2013.
[142] Seebauer, G. Edmund, Kratzer, C. Meredith, Charged Semiconductor Defects: Structure, Thermodynamics and Diffusion, Springer, Netherlands, 2009.
[143] D.A. Hanaor, C.C. Sorrell, Review of the anatase to rutile phase transformation, J. Mater. Sci. 46 (4) (2011) 855–874.
[144] M. Anpo, Utilization of TiO_2 photocatalysts in green chemistry, Pure Appl. Chem. 72 (7) (2000) 1265–1270.
[145] M. Anpo, et al., The design and development of second-generation titanium oxide photocatalysts able to operate under visible light irradiation by applying a metal ion-implantation method, Res. Chem. Intermed. 27 (4) (2001) 459–467.
[146] M. Anpo, S. Dohshi, M. Takeuchi, Preparation of Ti/B binary oxide thin films by the ionized cluster beam (ICB) method: their photocatalytic reactivity and photoinduced superhydrophilic properties, J. Ceram. Process. Res. 3 (4) (2002) 258–260.
[147] M. Anpo, M. Takeuchi, The design and development of highly reactive titanium oxide photocatalysts operating under visible light irradiation, J. Catal. 216 (1) (2003) 505–516.
[148] T. Umebayashi, et al., Analysis of electronic structures of 3d transition metal-doped TiO_2 based on band calculations, J. Phys. Chem. Solids 63 (10) (2002) 1909–1920.
[149] X. Nie, S. Zhuo, G. Maeng, K. Sohlberg, Doping of TiO_2 polymorphs for altered optical and photocatalytic properties, Int. J. Photoenergy (2009) 1–22.
[150] K. Kocí, et al., Effect of silver doping on the TiO_2 for photocatalytic reduction of CO_2, Appl. Catal. B 96 (3–4) (2010) 239–244.
[151] B. Xin, et al., Study on the mechanisms of photoinduced carriers separation and recombination for Fe^{3+}–TiO_2 photocatalysts, Appl. Surf. Sci. 253 (9) (2007) 4390–4395.
[152] A. Nishimura, G. Mitsui, M. Hirota, E. Hu, CO_2 reforming performance and visible light responsibility of Cr-doped TiO_2 prepared by sol–gel and dip-coating method, Int. J. Chem. Eng. (2010) 1–9.
[153] J.C.S. Wu, H.M. Lin, Photo reduction of CO_2 to methanol via TiO_2 photocatalyst, Int. J. Photoenergy 7 (3) (2005) 115–119.
[154] J. Wu, et al., Application of optical-fiber photoreactor for CO_2 photocatalytic reduction, Top. Catal. 47 (3) (2008) 131–136.
[155] O. Ola, et al., Performance comparison of CO_2 conversion in slurry and monolith photoreactors using Pd and Rh–TiO_2 catalyst under ultraviolet irradiation, Appl. Catal. B 126 (2012) 172–179.
[156] R. Asahi, T. Morikawa, Nitrogen complex species and its chemical nature in TiO_2 for visible-light sensitized photocatalysis, Chem. Phys. 339 (1–3) (2007) 57–63.
[157] M.M. Ren, Inverse opal titania on optical fiber for the photoreduction of CO_2 to CH_3OH, Int. J. Chem. Reactor Eng. 7 (2009) .
[158] M. Schiavello, Heterogeneous Photocatalysis, John Wiley & Sons, Chichester, 1997.
[159] E. Liu, et al., Photoconversion of CO_2 to methanol over plasmonic Ag/TiO_2 nano-wire films enhanced by overlapped visible-light-harvesting nanostructures, Ceram. Int. 41 (1) (2015) 1049–1057.
[160] B. Tahir, M. Tahir, N.S. Amin, Gold–indium modified TiO_2 nanocatalysts for photocatalytic CO_2 reduction with H_2 as reductant in a monolith photoreactor, Appl. Surf. Sci. 338 (2015) 1–14.
[161] S. Linic, P. Christopher, D.B. Ingram, Plasmonic-metal nanostructures for efficient conversion of solar to chemical energy, Nat. Mater. 10 (12) (2011) 911–921.
[162] M. Ovcharov, V. Shvalagin, V. Granchak, Photocatalytic reduction of carbon dioxide by water vapor on mesoporous titania modified by bimetallic Au/Cu nanostructures, Theory Exp. Chem. 50 (1) (2014) 53–58.
[163] T. Ohno, et al., Preparation of S-doped TiO_2 photocatalysts and their photocatalytic activities under visible light, Appl. Catal. A 265 (1) (2004) 115–121.
[164] K. Kondo, et al., Development of highly efficient sulfur-doped TiO_2 photocatalysts hybridized with graphitic carbon nitride, Appl. Catal. B 142 (2013) 362–367.
[165] J. Kim, W. Choi, H. Park, Effects of TiO_2 surface fluorination on photocatalytic degradation of methylene blue and humic acid, Res. Chem. Intermed. 36 (2) (2010) 127–140.
[166] C. Di Valentin, et al., N-doped TiO_2: theory and experiment, Chem. Phys. 339 (1) (2007) 44–56.
[167] C. Di Valentin, et al., Characterization of paramagnetic species in N-doped TiO_2 powders by EPR spectroscopy and DFT calculations, J. Phys. Chem. B 109 (23) (2005) 11414–11419.
[168] N. Serpone, et al., Spectroscopic, photoconductivity, and photocatalytic studies of TiO_2 colloids: naked and with the lattice doped with Cr^{3+}, Fe^{3+}, and V^{5+} cations, Langmuir 10 (3) (1994) 643–652.
[169] S. Rehman, et al., Strategies of making TiO_2 and ZnO visible light active, J. Hazard. Mater. 170 (2–3) (2009) 560–569.
[170] T. Morikawa, Y. Irokawa, T. Ohwaki, Enhanced photocatalytic activity of $TiO_{2-x}N_x$ loaded with copper ions under visible light irradiation, Appl. Catal. A 314 (1) (2006) 123–127.
[171] T. Morikawa, et al., Visible-light-induced photocatalytic oxidation of carboxylic acids and aldehydes over N-doped TiO_2 loaded with Fe, Cu or Pt, Appl. Catal. B 83 (1) (2008) 56–62.
[172] L. Huang, C. Sun, Y. Liu, Pt/N-codoped TiO_2 nanotubes and its photocatalytic activity under visible light, Appl. Surf. Sci. 253 (17) (2007) 7029–7035.
[173] Y. Cong, et al., Preparation, photocatalytic activity, and mechanism of nano-TiO_2Co-doped with nitrogen and iron(III), J. Phys. Chem. C 111 (28) (2007) 10618–10623.
[174] Q. Li, et al., Enhanced visible-light photocatalytic degradation of humic acid by palladium-modified nitrogen-doped titanium oxide, J. Am. Ceram. Soc. 90 (12) (2007) 3863–3868.
[175] L. Zhou, et al., Preparation and characterization of N–I co-doped nanocrystal anatase TiO_2 with enhanced photocatalytic activity under visible-light irradiation, Mater. Chem. Phys. 117 (2) (2009) 522–527.
[176] X. Yang, et al., Highly visible-light active C-and V-doped TiO_2 for degradation of acetaldehyde, J. Catal. 252 (2) (2007) 296–302.
[177] X. Yang, et al., Mixed phase titania nanocomposite codoped with metallic silver and vanadium oxide: new efficient photocatalyst for dye degradation, J. Hazard. Mater. 175 (1) (2010) 429–438.
[178] P. Richardson, et al., RETRACTED: manganese-and copper-doped titania nanocomposites for the photocatalytic reduction of carbon dioxide into methanol, Appl. Catal. B 126 (2012) 200–207.
[179] P. Richardson, et al., RETRACTED: heterogeneous photo-enhanced conversion of carbon dioxide to formic acid with copper-and gallium-doped titania nanocomposites, Appl. Catal. B 132 (2013) 408–415.
[180] X. Li, et al., Photocatalytic reduction of CO_2 over noble metal-loaded and nitrogen-doped mesoporous TiO_2, Appl. Catal. A 429 (2012) 31–38.
[181] Q. Zhang, et al., Copper and iodine co-modified TiO_2 nanoparticles for improved activity of CO_2 photoreduction with water vapor, Appl. Catal. B 123 (2012) 257–264.
[182] B.-J. Liu, T. Torimoto, H. Yoneyama, Photocatalytic reduction of CO_2 using surface-modified CdS photocatalysts in organic solvents, J. Photochem. Photobiol. A 113 (1) (1998) 93–97.
[183] Z.H. Zhao, et al., Optimal design and preparation of titania-supported CoPc using sol–gel for the photo-reduction of CO_2, Chem. Eng. J. 151 (1–3) (2009) 134–140.
[184] H.-Y. Wu, H. Bai, J.C. Wu, Photocatalytic Reduction of CO_2 using Ti-MCM-41 photocatalysts in monoethanolamine solution for methane production, Ind. Eng. Chem. Res. 53 (28) (2014) 11221–11227.
[185] A. Dhakshinamoorthy, et al., Photocatalytic CO_2 reduction by TiO_2 and related titanium containing solids, Energy Environ. Sci. 5 (11) (2012) 9217–9233.
[186] S. Kaneco, et al., Photocatalytic reduction of high pressure carbon dioxide using TiO_2 powders with a positive hole scavenger, J. Photochem. Photobiol. A 115 (3) (1998) 223–226.
[187] Z. Zhao, et al., Optimal design and preparation of titania-supported CoPc using sol–gel for the photo-reduction of CO_2, Chem. Eng. J. 151 (1) (2009) 134–140.
[188] K. Kočí, et al., Effect of temperature, pressure and volume of reacting phase on photocatalytic CO_2 reduction on suspended nanocrystalline TiO_2, Collect. Czech. Chem. Commun. 73 (8) (2008) 1192–1204.

[189] J.-M. Herrmann, Heterogeneous photocatalysis: fundamentals and applications to the removal of various types of aqueous pollutants, Catal. Today 53 (1) (1999) 115–129.
[190] H. Yamashita, et al., Photocatalytic synthesis of CH_4 and CH_3 OH from CO_2 and H_2O on highly dispersed active titanium oxide catalysts, Energy Convers. Manage. 36 (6) (1995) 617–620.
[191] F. Saladin, I. Alxneit, Temperature dependence of the photochemical reduction of CO_2 in the presence of H_2O at the solid/gas interface of TiO_2, J. Chem. Soc. Faraday Trans. 93 (23) (1997) 4159–4163.
[192] G. Guan, et al., Photoreduction of carbon dioxide with water over $K_2Ti_6O_{13}$ photocatalyst combined with Cu/ZnO catalyst under concentrated sunlight, Appl. Catal. A 249 (1) (2003) 11–18.
[193] Z.Y. Wang, et al., CO_2 photoreduction using NiO/$InTaO_4$ in optical-fiber reactor for renewable energy, Appl. Catal. A 380 (1–2) (2010) 172–177.
[194] S. Kaneco, et al., Photocatalytic reduction of CO_2 using TiO_2 powders in supercritical fluid CO_2, Energy 24 (1) (1999) 21–30.
[195] T. Mizuno, et al., Effect of CO_2 pressure on photocatalytic reduction of CO_2 using TiO_2 in aqueous solutions, J. Photochem. Photobiol. A 98 (1) (1996) 87–90.
[196] D. Erickson, D. Sinton, D. Psaltis, Optofluidics for energy applications, Nat. Photonics 5 (10) (2011) 583–590.
[197] R. Howe, Recent developments in photocatalysis, Dev. Chem. Eng. Mineral Process. 6 (1–2) (1998) 55–84.
[198] K. Koci, et al., Effect of TiO_2 particle size on the photocatalytic reduction of CO_2, Appl. Catal. B 89 (3–4) (2009) 494–502.
[199] C.B. Almquist, P. Biswas, Role of synthesis method and particle size of nanostructured TiO_2 on its photoactivity, J. Catal. 212 (2) (2002) 145–156.
[200] Z. Zhang, et al., Role of particle size in nanocrystalline TiO_2-based photocatalysts, J. Phys. Chem. B 102 (52) (1998) 10871–10878.
[201] A.N. Banerjee, The design, fabrication, and photocatalytic utility of nanostructured semiconductors: focus on TiO_2-based nanostructures, Nanotechnol. Sci. Appl. 4 (2011) 35.
[202] R.J. Braham, A.T. Harris, Review of major design and scale-up considerations for solar photocatalytic reactors, Ind. Eng. Chem. Res. 48 (19) (2009) 8890–8905.
[203] Y. Shioya, et al., Synthesis of transparent Ti-containing mesoporous silica thin film materials and their unique photocatalytic activity for the reduction of CO_2 with H_2O, Appl. Catal. A 254 (2) (2003) 251–259.
[204] K. Ikeue, et al., Photocatalytic reduction of CO_2 with H_2O on Ti-beta zeolite photocatalysts: Effect of the hydrophobic and hydrophilic properties, J. Phys. Chem. B 105 (35) (2001) 8350–8355.
[205] O. Kozák, et al., Preparation and characterization of ZnS nanoparticles deposited on montmorillonite, J. Colloid Interface Sci. 352 (2) (2010) 244–251.
[206] A.Y. Shan, T.I.M. Ghazi, S.A. Rashid, Immobilisation of titanium dioxide onto supporting materials in heterogeneous photocatalysis: a review, Appl. Catal. A 389 (1–2) (2010) 1–8.
[207] M. Dijkstra, et al., Comparison of the efficiency of immobilized and suspended systems in photocatalytic degradation, Catal. Today 66 (2) (2001) 487–494.
[208] Y.-H. Yu, et al., Photocatalytic NO reduction with C_3H_8 using a monolith photoreactor, Catal. Today 174 (1) (2011) 141–147.
[209] O. Ozcan, et al., Dye sensitized CO_2 reduction over pure and platinized TiO_2, Top. Catal. 44 (4) (2007) 523–528.
[210] E.G. Look, H.D. Gafney, Photocatalyzed conversion of CO_2 to CH_4: an excited-state acid–base mechanism, J. Phys. Chem. A 117 (47) (2013) 12268–12279.
[211] L. Liu, et al., Porous microspheres of MgO-patched TiO_2 for CO_2 photoreduction with H_2O vapor: temperature-dependent activity and stability, Chem. Commun. 49 (35) (2013) 3664–3666.
[212] J.Z. Tan, et al., Photoreduction of CO_2 using copper-decorated TiO_2 nanorod films with localized surface plasmon behavior, Chem. Phys. Lett. 531 (2012) 149–154.
[213] W.-N. Wang, et al., Size and structure matter: enhanced CO_2 photoreduction efficiency by size-resolved ultrafine Pt nanoparticles on TiO_2 single crystals, J. Am. Chem. Soc. 134 (27) (2012) 11276–11281.
[214] D. Chen, F. Li, A.K. Ray, Effect of mass transfer and catalyst layer thickness on photocatalytic reaction, AIChE J. 46 (5) (2000) 1034–1045.
[215] W. Choi, et al., Investigation on TiO_2-coated optical fibers for gas-phase photocatalytic oxidation of acetone, Appl. Catal. B 31 (3) (2001) 209–220.
[216] A. Danion, et al., Characterization and study of a single-TiO_2-coated optical fiber reactor, Appl. Catal. B 52 (3) (2004) 213–223.
[217] N.J. Peill, M.R. Hoffmann, Development and optimization of a TiO_2-coated fiber-optic cable reactor: photocatalytic degradation of 4-chlorophenol, Environ. Sci. Technol. 29 (12) (1995) 2974–2981.
[218] J. Xu, et al., Photocatalytic activity on TiO_2-coated side-glowing optical fiber reactor under solar light, J. Photochem. Photobiol. A 199 (2–3) (2008) 165–169.
[219] T.V. Nguyen, J.C.S. Yu, Photoreduction of CO_2 in an optical-fiber photoreactor: effects of metals addition and catalyst carrier, Appl. Catal. A 335 (1) (2008) 112–120.
[220] P. Du, et al., A novel photocatalytic monolith reactor for multiphase heterogeneous photocatalysis, Appl. Catal. A. 334 (1–2) (2008) 119–128.
[221] A.E. László Guczi, Catalysis for Alternative Energy Generation, Springer, New York, 2012.
[222] R.E. Marinangeli, D.F. Ollis, Photoassisted heterogeneous catalysis with optical fibers: I. Isolated single fiber, AIChE J. 23 (4) (1977) 415–426.
[223] H. Lin, K. Valsaraj, Development of an optical fiber monolith reactor for photocatalytic wastewater Treatment, J. Appl. Electrochem. 35 (7) (2005) 699–708.
[224] K. Nakata, A. Fujishima, TiO_2 photocatalysis: design and applications, J. Photochem. Photobiol. C 13 (3) (2012) 169–189.
[225] M. Tahir, N.S. Amin, Photocatalytic CO_2 reduction with H_2O vapors using montmorillonite/TiO_2 supported microchannel monolith photoreactor, Chem. Eng. J. 230 (2013) 314–327.
[226] M. Tahir, N.S. Amin, Photocatalytic CO_2 reduction and kinetic study over In/TiO_2 nanoparticles supported microchannel monolith photoreactor, Appl. Catal. A 467 (2013) 483–496.
[227] M. Singh, I. Salvadó-Estivill, G. Li Puma, Radiation field optimization in photocatalytic monolith reactors for air treatment, AIChE J. 53 (3) (2007) 678–686.
[228] M. Hossain, et al., Three-dimensional developing flow model for photocatalytic monolith reactors, AIChE J. 45 (6) (1999) 1309–1321.
[229] P.-Y. Liou, et al., Photocatalytic CO_2 reduction using an internally illuminated monolith photoreactor, Energy Environ Sci 4 (4) (2011) 1487–1494.
[230] O. Ola, M.M. Maroto-Valer, Copper based TiO_2 honeycomb monoliths for CO_2 photoreduction, Catal. Sci. Tech. 4 (6) (2014) 1631–1637.
[231] M.T. Merajin, et al., Photocatalytic conversion of greenhouse gases (CO_2 and CH_4) to high value products using TiO_2 nanoparticles supported on stainless steel webnet, J. Taiwan Inst. Chem. Eng. 44 (2) (2013) 239–246.
[232] A. Nishimura, et al., CO_2 reforming into fuel using TiO_2 photocatalyst and gas separation membrane, Catal. Today 148 (3–4) (2009) 341–349.
[233] P. Pathak, et al., Metal-coated nanoscale TiO_2 catalysts for enhanced CO_2 photoreduction, Green Chem. 7 (9) (2005) 667–670.
[234] A. Cybula, M. Klein, A. Zielińska-Jurek, M. Janczarek, A. Zaleska, Carbon dioxide photoconversion. The effect of titanium dioxide immobilization conditions and photocatalyst type, Physicochem. Prob. Mineral Process. 48 (1) (2012) 159–167.
[235] M.N. Chong, et al., Recent developments in photocatalytic water treatment technology: a review, Water Res. 44 (10) (2010) 2997–3027.
[236] M. Xing, F. Shen, B. Qiu, J. Zhang, Highly-dispersed boron-doped graphene nanosheets loaded with TiO_2 nanoparticles for enhancing CO_2 photoreduction, Sci. Rep. 4 (6341) (2014) 1–6.
[237] Q. Zhang, et al., Photoreduction of carbon dioxide by graphene–titania and zeolite–titania composites under low-intensity irradiation, Mater. Sci. Semicond. Process. 30 (2015) 162–168.
[238] E.S. Baeissa, Green synthesis of methanol by photocatalytic reduction of CO_2 under visible light using a graphene and tourmaline co-doped titania nanocomposites, Ceram. Int. 40 (8) (2014) 12431–12438.
[239] L.-L. Tan, et al., Noble metal modified reduced graphene oxide/TiO_2 ternary nanostructures for efficient visible-light-driven photoreduction of carbon dioxide into methane, Appl. Catal. B 166–167 (2015) 251–259.
[240] M.M. Gui, S.-P. Chai, A.R. Mohamed, Modification of MWCNT@TiO_2 core–shell nanocomposites with transition metal oxide dopants for photoreduction of carbon dioxide into methane, Appl. Surf. Sci. 319 (2014) 37–43.
[241] J. Low, et al., Two-dimensional layered composite photocatalysts, Chem. Commun. 50 (74) (2014) 10768–10777.
[242] W. Fan, Q. Zhang, Y. Wang, Semiconductor-based nanocomposites for photocatalytic H_2 production and CO_2 conversion, Phys. Chem. Chem. Phys. 15 (8) (2013) 2632–2649.
[243] W. Tu, et al., Robust hollow spheres consisting of alternating titania nanosheets and graphene nanosheets with high photocatalytic activity for CO_2 conversion into renewable fuels, Adv. Funct. Mater. 22 (6) (2012) 1215–1221.
[244] M.M. Gui, et al., Enhanced visible light responsive MWCNT/TiO_2 core–shell nanocomposites as the potential photocatalyst for reduction of CO_2 into methane, Sol. Energy Mater. Sol. Cells 122 (2014) 183–189.
[245] K.L. Choy, Chemical vapour deposition of coatings, Prog. Mater. Sci. 48 (2) (2003) 57–170.
[246] V. Galindo, et al., High quality $YBa_2Cu_3O_{7-\delta}$/$PrBa_2Cu_3O_{7-\delta}$ multilayers grown by pulsed injection MOCVD, J. Cryst. Growth 208 (1) (2000) 357–364.
[247] C. Ying, D. Hao, W. Lishi, Doped-TiO_2 photocatalysts and synthesis methods to prepare TiO_2 films, J. Mater. Sci. Technol. 24 (5) (2008) 675–689.
[248] X. Liu, et al., An improvement on sol–gel method for preparing ultrafine and crystallized titania powder, Mater. Sci. Eng. 289 (1–2) (2000) 241–245.
[249] V. Meille, Review on methods to deposit catalysts on structured surfaces, Appl. Catal. A 315 (2006) 1–17.
[250] U.G. Akpan, B.H. Hameed, The advancements in sol–gel method of doped-TiO_2 photocatalysts, Appl. Catal. A 375 (1) (2010) 1–11.
[251] C.-C. Wang, J.Y. Ying, Sol–gel synthesis and hydrothermal processing of anatase and rutile titania nanocrystals, Chem. Mater. 11 (11) (1999) 3113–3120.
[252] S. Sivakumar, et al., Nanoporous titania–alumina mixed oxides—an alkoxide free sol–gel synthesis, Mater. Lett. 58 (21) (2004) 2664–2669.
[253] Y. Li, T.J. White, S.H. Lim, Low-temperature synthesis and microstructural control of titania nano-particles, J. Solid State Chem. 177 (4–5) (2004) 1372–1381.
[254] J.C.S. Wu, I.H. Tseng, W.-C. Chang, Synthesis of titania-supported copper nanoparticles via refined alkoxide Sol–gel process, J. Nanoparticle Res. 3 (2) (2001) 113–118.
[255] C. Su, B.-Y. Hong, C.-M. Tseng, Sol–gel preparation and photocatalysis of titanium dioxide, Catal. Today 96 (3) (2004) 119–126.

[256] A. Nishimura, G. Mitsui, K. Nakamura, M. Hirota, E. Hu, CO_2 reforming characteristics under visible light response of Cr-or Ag-doped TiO_2 prepared by sol–gel and dip-coating process, Int. J. Photoenergy (2012) 1–12.
[257] M. Langlet, et al., Liquid phase processing and thin film deposition of titania nanocrystallites for photocatalytic applications on thermally sensitive substrates, J. Mater. Sci. 38 (19) (2003) 3945–3953.
[258] J. Zhang, et al., Importance of the relationship between surface phases and photocatalytic activity of TiO_2, Angew. Chem. Int. Ed. 47 (9) (2008) 1766–1769.
[259] B. Vijayan, et al., Effect of calcination temperature on the photocatalytic reduction and oxidation processes of hydrothermally synthesized titania nanotubes, J. Phys. Chem. C 114 (30) (2010) 12994–13002.
[260] K.L. Schulte, P.A. DeSario, K.A. Gray, Effect of crystal phase composition on the reductive and oxidative abilities of TiO_2 nanotubes under UV and visible light, Appl. Catal. B 97 (3) (2010) 354–360.
[261] J. Nair, et al., Microstructure and phase transformation behavior of doped nanostructured titania, Mater. Res. Bull. 34 (8) (1999) 1275–1290.
[262] G. Liu, et al., Engineering TiO_2 nanomaterials for CO_2 conversion/solar fuels, Sol. Energy Mater. Sol. Cells 105 (2012) 53–68.
[263] J.T. Carneiro, et al., How phase composition influences optoelectronic and photocatalytic properties of TiO_2, J. Phys. Chem. C 115 (5) (2011) 2211–2217.
[264] C.C. Yang, et al., Artificial photosynthesis over crystalline TiO_2-based catalysts: fact or fiction? J. Am. Chem. Soc. 132 (24) (2010) 8398–8406.
[265] A. Cybula, M. Klein, A. Zaleska, Methane formation over TiO_2-based photocatalysts: reaction pathways, Appl. Catal. B 164 (2015) 433–442.
[266] T. Yui, et al., Photochemical reduction of CO_2 using TiO_2: effects of organic adsorbates on TiO_2 and deposition of Pd onto TiO_2, ACS Appl. Mater. Interfaces 3 (7) (2011) 2594–2600.
[267] K. Teramura, et al., Photocatalytic conversion of CO_2 in water over layered double hydroxides, Angew. Chem. Int. Ed. 51 (32) (2012) 8008–8011.
[268] B.-J. Liu, et al., Effect of solvents on photocatalytic reduction of carbon dioxide using TiO_2 nanocrystal photocatalyst embedded in SiO_2 matrices, J. Photochem. Photobiol. A 108 (2–3) (1997) 187–192.
[269] Y. Fu, et al., An amine-functionalized titanium metal–organic framework photocatalyst with visible-light-induced activity for CO_2 reduction, Angew. Chem. Int. Ed. 51 (14) (2012) 3364–3367.
[270] T. Ohno, et al., Photocatalytic reduction of CO_2 over exposed-crystal-face-controlled TiO_2 nanorod having a brookite phase with co-catalyst loading, Appl. Catal. B 152 (2014) 309–316.
[271] T. Ohno, et al., Photocatalytic reduction of CO_2 over a hybrid photocatalyst composed of WO_3 and graphitic carbon nitride (g-C_3N_4) under visible light, J. CO_2 Util. 6 (2014) 17–25.
[272] C.W. Lee, R.A. Kourounioti, J.C. Wu, E. Murchie, M. Maroto-Valer, O.E. Jensen, A. Ruban, Photocatalytic conversion of CO_2 to hydrocarbons by light-harvesting complex assisted Rh-doped TiO_2 photocatalyst, J. CO_2 Util. 5 (2014) 33–40.
[273] P. Silija, Z. Yaakob, V. Suraja, N.N. Binitha, Z.S. Akmal, An enthusiastic glance in to the visible responsive photocatalysts for energy production and pollutant removal, with special emphasis on titania, Int. J. Photoenergy (2012) 1–19.
[274] K. Nishida, et al., In-situ monitoring of PE-CVD growth of TiO_2 films with laser Raman spectroscopy, Appl. Surf. Sci. 159 (2000) 143–148.
[275] C. Perego, S. Peratello, Experimental methods in catalytic kinetics, Catal. Today 52 (2–3) (1999) 133–145.
[276] T. Van Gerven, et al., A review of intensification of photocatalytic processes, Chem. Eng. Process. 46 (9) (2007) 781–789.
[277] H. Lin, An optical fiber monolith reactor for photocatalytic wastewater treatment, AIChE J. 52 (6) (2006) 2271–2280.
[278] R.-D. Sun, et al., TiO_2-coated optical fiber bundles used as a photocatalytic filter for decomposition of gaseous organic compounds, J. Photochem. Photobiol. A 136 (1–2) (2000) 111–116.
[279] M. Bouchy, O. Zahraa, Photocatalytic reactors, Int. J. Photoenergy 5 (3) (2003) 191–197.
[280] P.S. Mukherjee, Ray, Major challenges in the design of a large-scale photocatalytic reactor for water treatment, Chem. Eng. Technol. 22 (3) (1999) 253.
[281] A.K. Ray, Design, modelling and experimentation of a new large-scale photocatalytic reactor for water treatment, Chem. Eng. Sci. 54 (15) (1999) 3113–3125.
[282] J.-J. Wang, et al., Photocatalytic reduction of CO_2 to energy products using Cu–TiO_2/ZSM-5 and Co–TiO_2/ZSM-5 under low energy irradiation, Catal. Commun. 59 (2015) 69–72.
[283] B. Sánchez, et al., Influence of temperature on gas-phase photo-assisted mineralization of TCE using tubular and monolithic catalysts, Catal. Today 54 (2–3) (1999) 369–377.
[284] J.T. Carneiro, et al., An internally illuminated monolith reactor: pros and cons relative to a slurry reactor, Catal. Today 147 (Suppl. 1) (2009) S324–S329.
[285] W. Wang, The light transmission and distribution in an optical fiber coated with TiO_2 particles, Chemosphere 50 (8) (2003) 999–1006.
[286] J.C.S. Wu, H.-M. Lin, C.-L. Lai, Photo reduction of CO_2 to methanol using optical-fiber photoreactor, Appl. Catal. A 296 (2) (2005) 194–200.